



This discussion paper is/has been under review for the journal Atmospheric Chemistry and Physics (ACP). Please refer to the corresponding final paper in ACP if available.

An improved dust emission model with insights into the global dust cycle's climate sensitivity

J. F. Kok^{1,2}, N. M. Mahowald², S. Albani², G. Fratini^{3,*}, J. A. Gillies⁴, M. Ishizuka⁵, J. F. Leys⁶, M. Mikami⁷, M.-S. Park^{8,9}, S.-U. Park⁸, R. S. Van Pelt¹⁰, D. S. Ward², and T. M. Zobeck¹¹

¹Department of Atmospheric and Oceanic Sciences, University of California, Los Angeles, CA 90095, USA

²Department of Earth and Atmospheric Sciences, Cornell University, Ithaca, NY 14850, USA

³Department for innovation in biological, agro-food and forest systems (DIBAF), University of Tuscia, Via San Camillo de Lellis snc, 01100 Viterbo, Italy

⁴Division of Atmospheric Sciences, Desert Research Institute, 2215 Raggio Parkway, Reno NV 89512, USA

⁵Faculty of Engineering, Kagawa University, Takamatsu, Kagawa, 761-0396, Japan

⁶Science Division, Office of Environment and Heritage, Department of Premier and Cabinet, Gunnedah, New South Wales, Australia

⁷Japan Meteorological Research Institute, Tsukuba, Japan

An improved dust emission model

J. F. Kok et al.

Title Page

Abstract

Introduction

Conclusions

References

Tables

Figures

◀

▶

◀

▶

Back

Close

Full Screen / Esc

Printer-friendly Version

Interactive Discussion



⁸Center for Atmospheric and Environmental Modeling, Seoul National University Research Park RM. 515 San 4-2, Bongcheon-dong, Gwanak-gu, Seoul, 151-919, Korea

⁹Weather Information Service Engine Project, Center for Atmospheric Science & Earthquake Research, 12Fl. 434 Worldcupbukro Mapo-gu, Seoul, 121-835, Korea

¹⁰USDA-Agricultural Research Service, Wind Erosion and Water Conservation Research Unit, Big Spring, TX 79720, USA

¹¹USDA-Agricultural Research Service, Wind Erosion and Water Conservation Research Unit, Lubbock, TX, USA

* now at: LI-COR Biosciences GmbH, Siemensstr. 25A, 61352 Bad Homburg, Germany

Received: 12 December 2013 – Accepted: 21 February 2014 – Published: 11 March 2014

Correspondence to: J. F. Kok (jfkok@ucla.edu)

Published by Copernicus Publications on behalf of the European Geosciences Union.

An improved dust emission model

J. F. Kok et al.

Title Page

Abstract Introduction

Conclusions References

Tables Figures

◀ ▶

◀ ▶

Back Close

Full Screen / Esc

Printer-friendly Version

Interactive Discussion



Abstract

5 Simulations of the global dust cycle and its interactions with a changing Earth system are hindered by the empirical nature of dust emission parameterizations in climate models. Here we take a step towards improving global dust cycle simulations by presenting a physically-based dust emission model. The resulting dust flux parameterization depends only on the wind friction speed and the soil's threshold friction speed, and can therefore be readily implemented into climate models. We show that our parameterization's functional form is supported by a compilation of quality-controlled vertical dust flux measurements, and that it better reproduces these measurements than existing parameterizations. Both our theory and measurements indicate that many climate models underestimate the dust flux's sensitivity to soil erodibility. This finding can explain why dust cycle simulations in many models are improved by using an empirical preferential sources function that shifts dust emissions towards the most erodible regions. In fact, implementing our parameterization in a climate model produces even better agreement against aerosol optical depth measurements than simulations that use such a source function. These results indicate that the need to use a source function is at least partially eliminated by the additional physics accounted for by our parameterization. Since soil erodibility is affected by climate changes, our results further suggest that many models have underestimated the climate sensitivity of the global dust cycle.

1 Introduction

25 Mineral dust aerosols affect weather, climate, and the biosphere, including by scattering and absorbing radiation, altering cloud lifetime and reflectance, and serving as a nutrient source (Martin et al., 1991; Miller and Tegen, 1998; Forster et al., 2007). Conversely, the global dust cycle is highly sensitive to changes in climate (Tegen et al., 2004; Mahowald et al., 2006b; Washington et al., 2009), as evidenced both by global

ACPD

14, 6361–6425, 2014

An improved dust emission model

J. F. Kok et al.

Title Page

Abstract

Introduction

Conclusions

References

Tables

Figures

◀

▶

◀

▶

Back

Close

Full Screen / Esc

Printer-friendly Version

Interactive Discussion



An improved dust emission model

J. F. Kok et al.

Title Page

Abstract

Introduction

Conclusions

References

Tables

Figures

◀

▶

◀

▶

Back

Close

Full Screen / Esc

Printer-friendly Version

Interactive Discussion



dust deposition being several times larger during glacial maxima than during interglacials (Rea, 1994; Harrison et al., 2001) and by the apparent increase in global dust deposition over the past century (Prospero and Lamb, 2003; Mahowald et al., 2010). The radiative forcing resulting from such changes in the dust cycle might have played a critical role in amplifying past climate changes (Jansen et al., 2007), and may play an important role in present and future climate changes (Harrison et al., 2001; Mahowald et al., 2010).

Unfortunately, an accurate quantification of dust interactions with the Earth system in past and future climates is hindered by the empirical nature of dust emission parameterizations in climate models. Since these parameterizations are generally tuned to reproduce the current dust cycle (Ginoux et al., 2001; Zender et al., 2003a; Cakmur et al., 2006), applying them to a past or future climate, with substantial differences in global circulation and land surface, could produce large systematic errors. In particular, many dust modules in climate models use a *preferential sources function* (Ginoux et al., 2001; Tegen et al., 2002; Zender et al., 2003b; Grini et al., 2005; Koven and Fung, 2008) to account for global variations in *soil erodibility* (the ability of a soil to produce dust aerosols under a given wind stress in excess of the threshold stress needed to initiate dust emission (Zender et al., 2003b)). That is, the flux of dust emitted through wind erosion in a model grid cell is commonly represented by (Ginoux et al., 2001; Zender et al., 2003a; Grini et al., 2005)

$$\phi_d = C_{\text{tune}} S F_d, \quad (1)$$

where C_{tune} is a global tuning constant, usually set to maximize agreement against observations (Cakmur et al., 2006), and F_d is the vertical dust flux produced by an eroding soil per unit time and area, as predicted by a dust emission parameterization such as Gillette and Passi (1988) or Marticorena and Bergametti (1995) (hereafter GP88 and MB95, respectively). The preferential sources function S is a function of latitude and longitude, and usually shifts emissions towards the most erodible regions, such as North Africa (Ginoux et al., 2001; Tegen et al., 2002; Zender et al., 2003b).

An improved dust emission model

J. F. Kok et al.

Title Page

Abstract

Introduction

Conclusions

References

Tables

Figures

◀

▶

◀

▶

Back

Close

Full Screen / Esc

Printer-friendly Version

Interactive Discussion



The need to add a source function to improve agreement against observations was first noted by the pivotal study of Ginoux et al. (2001). They used the observation of Prospero et al. (2002) that dust “hot spots” tend to be co-located with topographic depressions to design a source function based on the relative height of a model grid cell compared to its surrounding cells. However, some subsequent studies challenged this inference by Prospero et al. (2002) because (i) the used remote sensing product is sensitive to boundary layer height, which tends to be higher over depressions in central desert regions (Mahowald and Dufresne, 2004), and because (ii) advection causes the remotely sensed dust loading to be shifted downwind from source regions (Schepanski et al., 2009). Nonetheless, the use of source functions, and the consequent shift of emissions towards regions with observed high dust loadings (Ginoux et al., 2001; Prospero et al., 2002), substantially improves model agreement with measurements (Zender et al., 2003b; Cakmur et al., 2006). This suggests that a key piece of physics is missing from existing parameterizations. And indeed, GP88 does not account for the effect of sediment availability or other soil properties on soil erodibility, and MB95 accounts for the soil erodibility using an empirical fit to data from a single study (Gillette, 1979). Since empirical parameterizations and source functions cannot accurately capture changes in soil erodibility produced by climate changes, which for instance affect soil moisture content and soil aggregation (Zobeck, 1991; Fecan et al., 1999; Kok et al., 2012; Shao, 2008), their use could cause substantial errors in model estimates of climate-induced changes in the global dust cycle.

Here we attempt to improve the global dust cycle’s representation in climate models, in particular for climate regimes other than the current climate to which most models are tuned (Cakmur et al., 2006). We do so by first presenting a physically-based theory for the vertical dust flux emitted by an eroding soil. The resulting parameterization is in better agreement with dust flux measurements than existing parameterizations in most climate models, and is relatively straightforward to implement since it uses only globally-available parameters. A critical insight from the theory is that the dust flux is substantially more sensitive to changes in the soil state than most climate

An improved dust emission model

J. F. Kok et al.

[Title Page](#)[Abstract](#)[Introduction](#)[Conclusions](#)[References](#)[Tables](#)[Figures](#)[I◀](#)[▶I](#)[◀](#)[▶](#)[Back](#)[Close](#)[Full Screen / Esc](#)[Printer-friendly Version](#)[Interactive Discussion](#)

models account for. The resulting underestimation of this sensitivity might explain why a source function that shifts emissions towards more erodible regions improves agreement against measurements. Indeed, we show that using our parameterization in a climate model produces better agreement against aerosol optical depth measurements than simulations that use a source function. Since soil erodibility is affected by climate changes, our results suggest that many models have underestimated the global dust cycle's climate sensitivity, and thus the radiative forcing resulting from the consequent change in atmospheric dust loading.

We derive our new dust emission parameterization in Sect. 2, after which we compare our parameterization's predictions against a compilation of quality-controlled vertical dust flux measurements in Sect. 3. In Sect. 4, we then test our parameterization's performance in a climate model by implementing it into the Community Earth System Model (CESM) and comparing the model predictions against measurements of aerosol optical depth by the AERosol RObotic NETwork (AERONET). We discuss the results and their implications for the dust cycle's climate sensitivity in Sect. 5, and finally summarize and conclude the article in Sect. 6.

2 Derivation of physically-based dust flux parameterization

Because of their small size, dust particles in soils ($< 62.5 \mu\text{m}$ diameter, Shao, 2008) experience cohesive forces that are large compared to aerodynamic and gravitational forces. Consequently, dust aerosols are usually not lifted directly by wind (Gillette et al., 1974; Shao et al., 1993; Sow et al., 2009) and instead are emitted through *saltation*, in which larger sand-sized particles ($\sim 70\text{--}500 \mu\text{m}$) move in ballistic trajectories (Bagnold, 1941; Shao, 2008; Kok et al., 2012). Upon impact, these saltating particles can eject dust particles from the soil, a process known as *sandblasting*. Moreover, some saltating particles are actually aggregates containing dust particles. Upon impact, these aggregates can also emit dust aerosols (Shao et al., 1996).

An improved dust emission model

J. F. Kok et al.

Title Page

Abstract

Introduction

Conclusions

References

Tables

Figures

◀

▶

◀

▶

Back

Close

Full Screen / Esc

Printer-friendly Version

Interactive Discussion



We aim to obtain an analytical expression that captures the main dependencies of the emitted flux of dust aerosols on wind speed and soil properties. An important limitation is that, to allow implementation into climate models, this expression can only use parameters that are globally available. Our approach to achieve this objective combines a theoretical derivation with numerical simulations of dust emission. We start by introducing the main variables used in the theory in the next section, after we derive the components of the analytical expression of the vertical dust flux in Sect. 2.2. We combine all these components together to give the full dust emission parameterization in Sect. 2.3.

2.1 Definition of main variables

The dust flux emitted by an eroding soil depends on the properties of the soil and on the wind shear stress τ exerted on the soil surface (Marticorena and Bergametti, 1995; Shao et al., 1996; Shao, 2001; Alfaro and Gomes, 2001; Klose and Shao, 2012; Kok et al., 2012). This shear stress is characterized by the friction velocity u'_* , which is a scaling parameter proportional to the velocity gradient in boundary layer flow, and is defined as (e.g., Bagnold, 1941; Shao, 2008; Kok et al., 2012)

$$u'_* = \sqrt{\tau/\rho_a}, \quad (2)$$

where ρ_a is the air density. Dust emission often occurs in the presence of non-erodible elements such as rocks and vegetation. Thus τ can be partitioned between the stress τ_R exerted on non-erodible roughness elements and the stress τ_S exerted on the bare soil; only τ_S produces dust emission (Raupach et al., 1993; Shao et al., 1996). In analogy with Eq. (2), we define the *soil friction velocity* corresponding to τ_S as

$$u_* = \sqrt{\frac{\tau_S}{f_{\text{bare}}\rho_a}}, \quad (3)$$

where f_{bare} is the fraction of the surface that consists of bare soil.

The *soil threshold friction velocity* u_{*t} is then the minimum value of u_* for which the bare soil experiences erosion. u_{*t} depends on both the properties of the fluid and on the gravitational and interparticle cohesion forces that oppose the fluid lifting of sand particles that initiates saltation (Kok et al., 2012; Shao and Lu, 2000). In principle, u_{*t} can be estimated from field measurements, as long as a correction is made for the presence of non-erodible elements, as discussed in the Supplement. However, the theoretical interpretation of this threshold is complicated by several factors. For instance, the threshold friction velocities at which saltation is initiated (the fluid or static threshold u_{*ft}) and terminated (the impact or dynamic threshold u_{*it}) are not equal. For most conditions, the impact threshold is thought to be smaller than the fluid threshold, of the order of $\sim 85\%$ (Bagnold, 1941; Kok, 2010). Moreover, spatial and temporal variations in soil conditions (Wiggs et al., 2004; Barchyn and Hugenholtz, 2011), as well as large variations in instantaneous wind speed for a given friction velocity (Rasmussen and Sorensen, 1999), make it such that there is generally not a clear value of u_* above which saltation does and below which it does not occur (Wiggs et al., 2004). Despite these problems, we neglect here for simplicity the temporal and spatial variability of u_{*t} and also assume that $u_{*t} = u_{*ft} = u_{*it}$, as previous dust emission parameterizations have also done (e.g., Gillette and Passi, 1988, Shao et al., 1996, Marticorena and Bergametti, 1995).

In addition to u_{*t} , we define the *standardized threshold friction velocity* (u_{*st}) as the value of u_{*t} at standard atmospheric density ($\rho_{a0} = 1.225 \text{ kg m}^{-3}$). Consequently, u_{*st} is not only independent of the presence of roughness elements, but is also invariant to variations in ρ_a , and is thus equal for similar soils at different elevations. Therefore, u_{*st} is a measure of the soil erodibility that depends on the state of the bare soil only. Since $u_{*t} \propto \sqrt{\rho_a}$ (e.g., Bagnold, 1941),

$$u_{*st} \equiv u_{*t} \sqrt{\rho_a / \rho_{a0}}. \quad (4)$$

An improved dust emission model

J. F. Kok et al.

Title Page

Abstract

Introduction

Conclusions

References

Tables

Figures

◀

▶

◀

▶

Back

Close

Full Screen / Esc

Printer-friendly Version

Interactive Discussion



An improved dust emission model

J. F. Kok et al.

Title Page

Abstract

Introduction

Conclusions

References

Tables

Figures

◀

▶

◀

▶

Back

Close

Full Screen / Esc

Printer-friendly Version

Interactive Discussion



We hypothesize that u_{*st} is a proxy for many of the soil properties known to affect dust emission, including soil cohesion, size distribution, and mineralogy (Fecan et al., 1999; Alfaro and Gomes, 2001; Shao, 2001). That is, although we do not understand in detail the effect of each of these soil properties on the dust flux (Shao, 2008), changes in soil properties that decrease the dust flux tend to also increase u_{*st} . Consequently, it is possible that u_{*st} can be used to partially account for the poorly understood effect of these soil properties on the dust flux.

2.2 Detailed theoretical expression of the vertical dust flux

The starting point of our theory is the insight that a saltator impact will produce dust emission only if a threshold impact energy is exceeded (Rice et al., 1999), with the nature and value of this threshold depending on the soil type and state. For instance, for a soil with only a small fraction of suspendable particles, much of the dust is present as coatings on larger sand particles (Bullard et al., 2004), such that the relevant threshold is likely the energy required for rupturing these coatings. Conversely, for a soil containing a large fraction of suspendable dust particles, the threshold for fragmentation of brittle dust aggregates could be most important (Kok, 2011b). Since the theoretical size distribution predicted by brittle fragmentation theory is in excellent agreement with measurements, the threshold for fragmentation of soil dust aggregates might be the most relevant threshold for dust emission under many conditions (Kok, 2011b). For simplicity, we thus assume that the energy required for dust aggregate fragmentation is globally the most relevant dust emission threshold, but we note that the functional form of the dust flux parameterization derived below is likely relatively insensitive to the chosen threshold process (see further discussion in Sect. 3.6). The vertical dust flux F_d ($\text{kg m}^{-2} \text{s}^{-1}$) generated by a soil during saltation can then be written as

$$F_d = f_{\text{bare}} n_s f_{\text{frag}} m_{\text{frag}} \mathcal{E}, \quad (5)$$

where f_{bare} is the fraction of the surface that consists of bare soil, n_s is the number of saltator impacts on the soil surface per unit area and time, f_{frag} is the average fraction

of saltator impacts resulting in fragmentation, m_{frag} is the mean mass of suspended dust produced per fragmenting impact, and ε is the mass fraction of emitted dust that does not reattach to the surface and is transported out of the near-surface layer where it can be measured (Gordon and McKenna Neuman, 2009). Since ε likely depends predominantly on the flow immediately above the surface, which remains relatively constant with wind speed (Ungar and Haff, 1987; Shao, 2008; Kok et al., 2012), we expect ε to be approximately constant for different wind conditions for a given soil. Finally, we obtain n_s from the balance of horizontal momentum in the saltation layer (Shao et al., 1996),

$$n_s = \frac{C_{\text{ns}} \rho_a (u_*^2 - u_{*t}^2)}{m_s \overline{v_{\text{imp}}}}, \quad (6)$$

where the constant $C_{\text{ns}} \approx 2$ (Kok et al., 2012), and m_s and $\overline{v_{\text{imp}}}$ are the mean saltator mass and impact speed. Substituting Eq. (6) into Eq. (5) yields

$$F_d = f_{\text{bare}} f_{\text{clay}} \gamma \varepsilon \frac{C_{\text{ns}} \rho_a (u_*^2 - u_{*t}^2)}{\overline{v_{\text{imp}}}} f_{\text{frag}}, \quad (7)$$

where we assumed that $m_{\text{frag}}/m_s = \gamma f_{\text{clay}}$. That is, we assumed that m_{frag}/m_s scales with the volume fraction of the soil that contributes to the creation of dust aerosols (Sweeney and Mason, 2013). The size limit of dust relevant for climate is usually taken as $\sim 10 \mu\text{m}$ (Mahowald et al., 2010, 2006b), but since the mass fraction of soil particles $\leq 10 \mu\text{m}$ is not available on a global scale, we instead use the soil clay fraction (f_{clay} ; $\leq 2 \mu\text{m}$ diameter), which is globally available (FAO, 2012). The dimensionless coefficient γ depends on the relative sizes of dust aggregates and saltators. Because many saltators are aggregates (Shao, 2008), we expect only modest variations in γ between soils and take it as a constant.

An improved dust emission model

J. F. Kok et al.

Title Page

Abstract

Introduction

Conclusions

References

Tables

Figures

◀

▶

◀

▶

Back

Close

Full Screen / Esc

Printer-friendly Version

Interactive Discussion



An improved dust emission model

J. F. Kok et al.

Title Page

Abstract

Introduction

Conclusions

References

Tables

Figures

◀

▶

◀

▶

Back

Close

Full Screen / Esc

Printer-friendly Version

Interactive Discussion



Since we expect variations of γ and ε with wind and soil conditions to be less important (see above), we need to understand the dependence of $\overline{v_{\text{imp}}}$ and f_{frag} on u_* and u_{*st} in order to obtain the dust flux's dependence on u_* and u_{*st} . We derive the dependencies of $\overline{v_{\text{imp}}}$ and f_{frag} on u_* and u_{*st} in the following sections through a combination of theory and simulations with the numerical saltation model COMSALT (Kok and Renno, 2009).

2.2.1 The mean saltator impact speed ($\overline{v_{\text{imp}}}$)

After saltation has been initiated by the aerodynamic lifting of surface particles, new particles are brought into saltation primarily through the ejection, or splashing, of surface particles by impacting saltators (Ungar and Haff, 1987; Duran et al., 2011; Kok et al., 2012;). (Note that this is only correct for soils with a sufficient supply of loose sand particles. The present theory is not valid for soils that instead are *supply-limited*, which we discuss in further detail in Sect. 3.6) Saltation is thus in steady state when exactly one particle is ejected from the soil bed for each particle impacting it. Since the number of splashed particles increases with the impacting saltator's speed (Kok et al., 2012), this condition for steady state is met at a particular value of $\overline{v_{\text{imp}}}$. Consequently, theory and measurements indicate that $\overline{v_{\text{imp}}}$ is independent of u_* for steady-state saltation (Duran et al., 2011; Kok, 2011a; Kok et al., 2012; Ungar and Haff, 1987) (Supplement Fig. S1).

Although $\overline{v_{\text{imp}}}$ is independent of u_* , it does depend on soil properties. In particular, the soil's saltation threshold sets the wind speed in the near-surface layer (Bagnold, 1941), which in turn determines the particle speed (Duran et al., 2011; Kok et al., 2012). To first order then,

$$\overline{v_{\text{imp}}} = C_v u_{*st}, \quad (8)$$

where $C_v \approx 5$ since $\overline{v_{\text{imp}}} \approx 1 \text{ ms}^{-1}$ for loose sand with $u_{*st} \approx 0.20 \text{ ms}^{-1}$ (Supplement Fig. S1).

2.2.2 The fragmentation fraction (f_{frag})

An impacting saltator can fragment a dust aggregate in the soil if its impact energy exceeds a certain threshold (Kun and Herrmann, 1999; Kok, 2011b). The threshold impact energy per unit area ψ (Jm^{-2}) required to fragment a soil dust aggregate scales with the sum of the energetic cohesive bonds E_{coh} between the constituent particles that make up the aggregate (Kun and Herrmann, 1999). That is,

$$\psi \propto \sum E_{\text{coh}}/D_s^2, \quad (9)$$

where D_s is the saltator size, and the sum is over all interparticle bonds in the aggregate. Measurements and theory suggest that (Shao, 2001)

$$E_{\text{coh}} \propto \beta D_c^2, \quad (10)$$

where D_c is the typical size of a constituent particle of the dust aggregate. The parameter β (Jm^{-2}) scales the interparticle force, which is the sum of a complex collection of individual forces, including van der Waals, water adsorption, and electrostatic forces (Shao and Lu, 2000). Consequently, β depends on the state of the soil, including soil moisture content, mineralogy, and size distribution. Since the number of bonds in the aggregate scales with D_{ag}^3/D_c^3 , where D_{ag} is the aggregate size, Eq. (9) becomes

$$\psi \propto \beta D_{\text{ag}}^3 / (D_s^2 D_c), \quad (11)$$

For highly erodible, dry soils, $\beta = \beta_0 \approx 1.5 \times 10^{-4} \text{Jm}^{-2}$ (Shao and Lu, 2000; Kok and Renno, 2006). Experiments suggest that most typical saltator impacts (i.e., $D_s = 100 \mu\text{m}$ and $v_{\text{imp}} = 1 \text{ms}^{-1}$) eject dust for such highly erodible, dry soils (Rice et al., 1996), yielding $\psi_0 \approx 0.1 \text{Jm}^{-2}$. Thus,

$$\tilde{\psi} = c_{\psi} \tilde{\beta}, \quad (12)$$

Title Page

Abstract

Introduction

Conclusions

References

Tables

Figures

◀

▶

◀

▶

Back

Close

Full Screen / Esc

Printer-friendly Version

Interactive Discussion



An improved dust emission model

J. F. Kok et al.

Title Page

Abstract

Introduction

Conclusions

References

Tables

Figures

◀

▶

◀

▶

Back

Close

Full Screen / Esc

Printer-friendly Version

Interactive Discussion



where $\tilde{\psi} = \psi/\psi_0$ and $\tilde{\beta} = \beta/\beta_0$. The dimensionless parameter c_ψ is of order unity and depends on the soil size distribution since it scales with $D_{ag}^3/(D_s^2 D_c)$. In particular, because saltators are often aggregates (Shao, 2008), with both D_{ag} and D_s having typical sizes of the order of 100 μm (Shao, 2001), the leading order scaling is likely $c_\psi \sim D_{ag}/D_c$. Here we take c_ψ as a constant, both because there are insufficient vertical dust flux data sets available that report a detailed soil size distribution, and because global soil data sets are not nearly detailed enough to represent spatial and temporal variability in the soil size distribution.

Since the soil's standardized threshold friction velocity (u_{*st}) depends on the strength of interparticle forces (Shao and Lu, 2000), ψ must increase monotonically with u_{*st} (Shao et al., 1996). This is intuitive: soils that are more erosion resistant, for example with strongly-bound soil aggregates due to surface crusts or high moisture content, require a larger impact energy to fragment (Rice et al., 1996, 1999). For such soils, wind tunnel experiments show that only a small fraction of saltator impacts produce dust emission (Rice et al., 1996).

We calculate the fragmentation fraction f_{frag} from the overlap between the probability distributions of ψ and the saltator impact energy per unit area E_{imp} . Since ψ is the sum of a large number of individual cohesive bonds, its probability distribution $P_\psi(\psi)$ is normally distributed per the central limit theorem (Kallenberg, 1997), with a mean $\bar{\psi}$ and standard deviation σ_ψ . The total fraction of saltator impacts that produces dust emission through fragmentation then equals

$$\begin{aligned}
 f_{frag} &= \int_0^\infty \int_0^{E_{imp}} P_{E_{imp}}(E_{imp}) P_\psi(\psi) d\psi dE_{imp} \\
 &= \int_0^\infty P_{E_{imp}}(E_{imp}) \left\{ \frac{1}{2} + \frac{1}{2} \operatorname{erf} \left[\frac{E_{imp} - \bar{\psi}}{\sqrt{2}\sigma_\psi} \right] \right\} dE_{imp},
 \end{aligned} \tag{13}$$

where erf is the error function, which results from the integration of the normally-distributed ψ .

Determining the $P_{E_{\text{imp}}}$ with the numerical saltation model COMSALT

In order to calculate f_{frag} with Eq. (13), we require the probability distribution of saltator impact energies ($P_{E_{\text{imp}}}$) for given values of u_* , β , and D_s , which we obtain through simulations with the numerical saltation model COMSALT (Kok and Renno, 2009). This model explicitly simulates the trajectories of saltators due to gravitational and fluid forces, and accounts for the stochasticity of individual particle trajectories due to turbulence and collisions with the irregular soil surface. Moreover, COMSALT simulates the retardation of the wind profile by the drag of saltating particles, which is the process that ultimately limits the number of particles that can be saltating at any given time. Finally, in contrast to many previous models, COMSALT includes a physically-based parameterization of the ejection (“splashing”) of surface particles, based on conservation of energy and momentum (Kok and Renno, 2009). Because of this explicit inclusion of splash, as well as other improvements over previous studies, COMSALT is the first numerical model capable of reproducing a wide range of measurements of naturally occurring saltation.

Since COMSALT was developed for saltation of soils made up of loose sand, it must be adapted in order to simulate saltation over dust-emitting soils. For soils made up of loose sand, the splashing of new saltating particles is constrained predominantly by the momentum transferred by impacting saltators (Kok and Renno, 2009). That is, the total momentum of splashed particles scales with the impacting saltator momentum (Beladjine et al., 2007; Oger et al., 2008). For dust emitting soils, this situation is likely different, because saltating particles are more strongly bound in the soil by cohesive forces (Shao and Lu, 2000; Kok and Renno, 2009). We therefore assume that, for dust emitting soils, the number of particles splashed by an impacting saltator scales with its impacting energy (Shao and Li, 1999). Furthermore, in order for a saltating particle to eject another saltator from the soil, the impact must be sufficiently energetic

An improved dust emission model

J. F. Kok et al.

Title Page

Abstract

Introduction

Conclusions

References

Tables

Figures

◀

▶

◀

▶

Back

Close

Full Screen / Esc

Printer-friendly Version

Interactive Discussion



to overcome the cohesive the bonds with other soil particles. Therefore, the larger the soil cohesive forces, the stronger the cohesive binding energy $E_{\text{coh},s}$ with which sand-sized particles are bonded to other soil particles, resulting in a smaller number of splashed saltating particles N . That is,

$$N \propto \frac{m_s v_{\text{imp}}^2 / 2}{E_{\text{coh},s}}, \quad (14)$$

Since $E_{\text{coh},s}$ scales with βD_s^2 (see Eq. 10 and Shao, 2001), Eq. (11) becomes

$$N = a_E \frac{\rho_p D_s v_{\text{imp}}^2}{\beta}, \quad (15)$$

where the dimensionless parameter a_E scales the number of splashed particles. We obtain $a_E = 6.1 \times 10^{-5}$ by forcing the minimum u_* for which saltation can occur in COMSALT with $\beta = \beta_0$ to equal the minimal value of u_{*st} for an optimally erodible soil. We define this minimal value as u_{*st0} , and measurements show that $u_{*st0} \sim 0.16 \text{ m s}^{-1}$ for a bed of $100 \mu\text{m}$ loose sand particles (Bagnold, 1941; Iversen and White, 1982; Kok et al., 2012).

Other parameters of the splash process, such as the speed of splashed particles, the coefficient of restitution, and the probability that an impacting saltator does not rebound, are treated as described in Kok and Renno (2009). We thus neglect any change in these parameters with changes in soil cohesion since there is very little experimental data available to account for any such dependences (O'Brien and McKenna Neuman, 2012). COMSALT also computes the soil's standardized threshold friction velocity u_{*st} as the minimum value of u_* at which saltation can be sustained for a given value of β , following the procedure outlined in Kok and Renno (2009).

COMSALT simulations of $P_{E_{\text{imp}}}$ show that, although the mean saltator impact speed $(\overline{v_{\text{imp}}})$ remains approximately constant with u_* (see above), the distribution of E_{imp} does

not (Fig. 1). Because the total drag exerted by saltators on the flow increases with u_* , the wind profile lower in the saltation layer is relatively insensitive to u_* (Owen, 1964; Ungar and Haff, 1987; Duran et al., 2011; Kok et al., 2012). Conversely, the wind speed higher up in the saltation layer does increase with u_* (Bagnold, 1941), which causes the speed and abundance of energetic particles moving higher in the saltation layer to also increase. This causes a non-linear increase in the high-energy tail of $P_{E_{\text{imp}}}$ with u_* (Fig. 1; also see Duran et al., 2011 and Kok et al., 2012).

Dependence of f_{frag} on u_* and u_{*st}

Since we can obtain $P_{E_{\text{imp}}}$ for given values of u_* , D_s , and β (and thus u_{*st}) from COMSALT simulations, we can use Eq. (13) to determine f_{frag} for given values of c_ψ and σ_ψ . Given that the exact values of c_ψ and σ_ψ for any particular soil are unknown, our objective in using Eq. (13) is to understand the functional form of the dependence of f_{frag} , and thus F_d , on u_* and u_{*st} . To understand these dependencies, we consider the distributions of E_{imp} and ψ for two limiting cases: a highly erodible and an erosion-resistant soil (Fig. 1). For a highly erodible soil, a large fraction of saltator impacts can be expected to produce fragmentation (Rice et al., 1996 and Fig. 1a), such that $\overline{E_{\text{imp}}} \sim \overline{\psi}$. In this case, the value of f_{frag} is thus approximately constant with u_* (Fig. 1c). Conversely, when the soil is erosion-resistant, $\overline{E_{\text{imp}}} \ll \overline{\psi}$, and only the high-energy tail of the impact energy distribution results in dust emission through fragmentation (Fig. 1b). Since this high-energy tail increases sharply with u_* , f_{frag} also increases sharply with u_* (Fig. 1c). Consequently, F_d scales more strongly with u_* for erosion-resistant than for highly erodible soils.

Our results thus show that f_{frag} depends on both u_* and u_{*st} (Fig. 1c). Since f_{frag} is dimensionless, its dependency on u_* and u_{*st} should take the form of the non-dimensional ratios that capture the physical processes determining f_{frag} (Buckingham, 1914). That is, f_{frag} should depend only on (i) the dimensionless friction velocity u_*/u_{*st} , which sets the increase of the high-energy tail (Fig. 1), and (ii) the dimensionless stan-

Title Page

Abstract

Introduction

Conclusions

References

Tables

Figures

◀

▶

◀

▶

Back

Close

Full Screen / Esc

Printer-friendly Version

Interactive Discussion



standardized threshold velocity u_{*st}/u_{*st0} , which sets the erodibility of the soil. From Fig. 1c, we infer

$$f_{frag} = C_{fr} \left(\frac{u_*}{u_{*t}} \right)^\alpha. \quad (16)$$

5 Since this power law accounts for the dependence of f_{frag} on u_*/u_{*t} , the dimensionless fragmentation constant C_{fr} and exponent α must depend only on the other dimensionless number, u_{*st}/u_{*st0} (Buckingham, 1914). Since highly erodible soils with $u_{*st} = u_{*st0}$ have $\alpha \approx 0$ (Fig. 1), we hypothesize that

$$10 \quad \alpha = C_\alpha \left(\frac{u_{*st} - u_{*st0}}{u_{*st0}} \right), \quad (17)$$

where C_α is a dimensionless constant. Equation (17) is supported by numerical simulations of f_{frag} for a range of plausible values of the saltator diameter D_s and the threshold fragmentation energy's normal distribution parameters (Fig. 2a).

15 The proportionality constant C_{fr} in Eq. (16) must decrease sharply with u_{*st} (Fig. 1c), because increases in u_{*st} are primarily driven by increases in soil (aggregate) cohesion (Kok et al., 2012; Shao, 2008; Shao and Lu, 2000), for instance due to increases in soil moisture. Such increases in aggregate cohesion reduce the fragmentation fraction f_{frag} , and numerical simulations indicate that (Fig. 2b)

$$20 \quad C_{fr} = C_{fr0} \exp \left(-C_e \frac{u_{*st} - u_{*st0}}{u_{*st0}} \right), \quad (18)$$

where $C_{fr0} \approx 0.5$ is the fragmentation fraction for highly erodible soils (Fig. 1c), and C_e is a dimensionless constant.

An improved dust emission model

J. F. Kok et al.

| | |
|--------------------------|--------------|
| Title Page | |
| Abstract | Introduction |
| Conclusions | References |
| Tables | Figures |
| ◀ | ▶ |
| ◀ | ▶ |
| Back | Close |
| Full Screen / Esc | |
| Printer-friendly Version | |
| Interactive Discussion | |



2.3 Full theoretical expression for the vertical dust flux

We complete our theoretical expression by substituting Eqs. (8) and (16)–(18) into Eq. (7), yielding

$$F_d = C_d f_{\text{bare}} f_{\text{clay}} \frac{\rho_a (u_*^2 - u_{*t}^2)}{u_{*st}} \left(\frac{u_*}{u_{*t}} \right)^{C_\alpha \frac{u_{*st} - u_{*st0}}{u_{*st0}}}, \quad (19a)$$

where

$$C_d = C_{d0} \exp \left(-C_e \frac{u_{*st} - u_{*st0}}{u_{*st0}} \right), \quad (19b)$$

with $C_{d0} = \gamma \varepsilon C_{\text{ns}} C_{\text{fr0}} / C_v$. Equation (19) thus predicts that F_d scales with u_* to the power $a \equiv \alpha + 2$. The dimensionless dust emission coefficient C_d is independent of u_* , and is thus a measure of soil erodibility. More specifically, it quantifies the soil's susceptibility to erosion under saltation bombardment. We determine the dimensionless coefficients C_α , C_e , and C_{d0} through comparison against a quality-controlled compilation of vertical dust flux data sets in Sect. 3.

The decrease in the dust emission coefficient C_d with increasing u_{*st} accounts for a soil's reduced ability to produce dust under saltation bombardment as the soil erodibility decreases. This is an important result, as this process is not included in the previous dust flux parameterizations of GP88 and MB95 that dominate dust modules in current climate models (e.g., Ginoux et al., 2001, Zender et al., 2003a). In particular, it implies that the dust flux is more sensitive to soil erodibility than climate models currently account for. We discuss this result and its implications further in Sect. 5.

Note that the dust flux parameterization of Eq. (19) is simpler than previous physically-based dust emission models (Shao, 2001; Shao et al., 1996). Since its main parameters (u_* , u_{*t} , and f_{clay}) are available in climate models, its implementation in models is relatively straightforward.

Title Page

Abstract

Introduction

Conclusions

References

Tables

Figures

◀

▶

◀

▶

Back

Close

Full Screen / Esc

Printer-friendly Version

Interactive Discussion



3 Assessment of parameterization performance using a quality-controlled compilation of dust flux measurements

We test our proposed dust emission parameterization using a compilation of quality-controlled literature data sets. We do so by first separately testing the two main improvements of Eq. (19) over previous theories: the linear increase of the dust emission coefficient a with u_{*st} , and the exponential decrease of the dust emission coefficient C_d with u_{*st} . This procedure also yields estimates of the dimensionless parameters C_α , C_{d0} , and C_θ , subsequently allowing us to directly compare the measured dust flux against the predictions of Eq. (19).

The following section discusses the quality-control criteria that data sets need to meet in order to allow an accurate comparison against our theoretical expression. Section 3.2 then describes the various corrections applied to bring all data sets on an equal footing, after which Sect. 3.3 describes the procedure for determining the dust emission coefficient (C_d) and fragmentation exponent (α) from literature data sets of dust flux measurements. We then test the functional form of the parameterization against the estimates of C_d and α extracted from the literature data sets in Sect. 3.4, and test the parameterization's predictions of the vertical dust flux against our dust flux compilation in Sect. 3.5. Finally, we discuss some limitations of our parameterization in Sect. 3.6.

3.1 Data set quality-control criteria

We strive to obtain a compilation of high-quality vertical dust flux measurements that we can use to test our new parameterization. We thus apply several quality-control criteria that data sets need to meet in order to be included in our compilation; these criteria are designed to ensure that the measured dust flux is governed by a soil in an approximately constant state. This is critical, because any changes in the soil state affects u_{*t} , which is one of the main parameters in our parameterization. Since changes in the threshold friction velocity can occur on timescales as short as an hour (Barchyn

[Title Page](#)[Abstract](#)[Introduction](#)[Conclusions](#)[References](#)[Tables](#)[Figures](#)[◀](#)[▶](#)[◀](#)[▶](#)[Back](#)[Close](#)[Full Screen / Esc](#)[Printer-friendly Version](#)[Interactive Discussion](#)

An improved dust emission model

J. F. Kok et al.

Title Page

Abstract

Introduction

Conclusions

References

Tables

Figures

◀

▶

◀

▶

Back

Close

Full Screen / Esc

Printer-friendly Version

Interactive Discussion



and Hugenholtz, 2011; Wiggs et al., 2004), we only use data sets for which all data was taken within a limited time period of up to ~ 12 h. This requirement excludes many of the data sets on which previous dust flux schemes were based, in particular data sets by Gillette (1979), Nickling and colleagues (Nickling, 1978, 1983; Nickling and Gillies, 1993; Nickling et al., 1999), and Gomes et al. (2003). In addition, we require that a data set contains sufficient measurements to reliably determine the threshold friction velocity for the measurements. Furthermore, we only use data sets of natural dust emission taken in the field, because the characteristics of saltation and dust emission simulated in (portable) wind tunnels have been shown to, in some cases, be substantially different from the characteristics of natural saltation (Sherman and Farrell, 2008; Kok, 2011a). Finally, the measurements should be made for relatively homogeneous terrain, such that the soil state is spatially approximately constant. This last constraint is only required for predicting the dust emission coefficient C_d . Therefore, data sets that meet all criteria except that of homogeneous terrain (i.e., the data sets of Fratini et al., 2007 and Park et al., 2011) are not used for comparison against the theoretical equations for C_d and F_d , but are still used for assessing the fragmentation exponent α .

Our literature search for vertical dust flux measurements that met the above quality-control criteria resulted in the identification of 6 studies: Gillies and Berkofsky (2004) (hereinafter referred to as GB04), Zobeck and Van Pelt (2006) (ZP06), Fratini et al. (2007) (FC07), Sow et al. (2009) (SA09), Shao et al. (2011) (SI11), and Park et al. (2011) (PP11). Images of the experimental sites of these 6 studies are shown in Fig. 3, and the main properties of each data set are summarized in Table 1. We used the original data for each of these 6 studies, and extracted 11 individual data sets from them. We describe the general procedures for correcting for differences between data sets and for extracting estimates of u_{*t} , α , and C_d in the next two sections. A detailed description of the analysis of each individual data set is provided in the Supplement.

3.2 Correcting for differences in averaging period and measured size range

A critical property of dust flux data sets is the time period over which measurements are averaged. In particular, since the vertical dust flux is non-linear in the friction velocity, the averaging period needs to be consistent among data sets (Sow et al., 2009; Martin et al., 2013). In setting the averaging period, an important consideration is that the friction velocity, being a turbulence parameter, is only meaningful when obtained over averaging periods long enough to sample a sufficient range of the turbulent eddies contributing to the downward flux of horizontal fluid momentum (Kaimal and Finnigan, 1994; Namikas et al., 2003; van Boxel et al., 2004). Moreover, the averaging period needs to be short enough such that the meteorological forcing of the boundary layer, which partially sets the downward momentum transfer, remains approximately constant. A compromise between these constraints is an averaging period of 30 min (Goulden et al., 1996; Aubinet et al., 2001; van Boxel et al., 2004; Fratini et al., 2007), which conveniently is also of the order of the typical time step in global models. We thus reanalyzed each data set using a 30 min averaging period. In order to get maximum use out of each data set, the data were averaged over 30 min with a running average (e.g., a 60 min continuous data set with 1 min resolution yielded 31 data points).

In addition to using the same averaging period for each data set, we also need to correct for differences in the measured dust size range between the data sets. We therefore corrected each data set to represent the mass flux of dust aerosols with a geometric diameter D_d between 0–10 μm , which is a size range commonly represented in atmospheric circulation models (Mahowald et al., 2006b). Several of the dust flux data sets (e.g., GB04, ZP06) reported size ranges not in terms of the geometric diameter D_d , which is defined as the diameter of a sphere having the same volume as the irregularly-shaped dust aerosol, but in terms of the aerodynamic diameter, D_{ae} , which is defined as the diameter of a spherical particle with density $\rho_0 = 1000 \text{ kg m}^{-3}$ with the same aerodynamic resistance as the dust aerosol (Hinds, 1999). Therefore, depending on the data set, two separate corrections need to be made: one to correct from aero-

An improved dust emission model

J. F. Kok et al.

[Title Page](#)[Abstract](#)[Introduction](#)[Conclusions](#)[References](#)[Tables](#)[Figures](#)[◀](#)[▶](#)[◀](#)[▶](#)[Back](#)[Close](#)[Full Screen / Esc](#)[Printer-friendly Version](#)[Interactive Discussion](#)

dynamic diameter to geometric diameter, and one to correct the measured geometric size range to 0–10 μm .

The geometric and aerodynamic diameters are related by (Hinds, 1999; Reid et al., 2003)

$$D_d = \sqrt{\frac{\chi \rho_0}{\rho_p}} D_{ae}, \quad (20)$$

where $\rho_p \approx 2.5 \pm 0.2 \times 10^3 \text{ kg m}^{-3}$ is the typical density of a dust aerosol particle (Kaaden et al., 2009), and χ is the dynamic shape factor, which is defined as the ratio of the drag force experienced by the irregular particle to the drag force experienced by a spherical particle with diameter D_d (Hinds, 1999). Measurements of the dynamic shape factor for mineral dust particles with a geometric diameter of $\sim 10 \mu\text{m}$ find $\chi \approx 1.4 \pm 0.1$ (Cartwright, 1962; Davies, 1979; Kaaden et al., 2009). Inserting this into Eq. (20) then yields that $D_d \approx (0.75 \pm 0.04) D_{ae}$, where the standard error was obtained using error propagation (Bevington and Robinson, 2003).

After converting each data set's measured aerodynamic particle size range to a geometric size range as necessary, we corrected the measured dust flux by assuming that the size distribution at emission is well-described by the theoretical dust size distribution expression of Kok (2011b), which is in excellent agreement with measurements. For instance, Eq. (6) in Kok (2011b) predicts that $71 \pm 5\%$ of emitted dust in the geometric 0–10 μm size range lies in the aerodynamic 0–10 μm size range (which is equivalent to the geometric $0-7.5 \pm 0.4 \mu\text{m}$ size range). We thus apply a correction factor of $(0.71 \pm 0.05)^{-1} = 1.42 \pm 0.10$ in order to correct a measured aerodynamic PM_{10} flux (e.g., GB04, ZP06) to a geometric $\leq 10 \mu\text{m}$ flux. Note that the uncertainty in the correction factor is propagated into the uncertainty on the value of C_d extracted from each data set (see the Supplement).

In addition to correcting for differences between data sets in the averaging time and the measured size range, we also corrected for differences in the fetch length when possible (see Supplement text).

An improved dust emission model

J. F. Kok et al.

Title Page

Abstract

Introduction

Conclusions

References

Tables

Figures

◀

▶

◀

▶

Back

Close

Full Screen / Esc

Printer-friendly Version

Interactive Discussion



3.3 Procedure for obtaining u_{*t} , α , and C_d

After putting all data on an equal footing using the above procedures, we can extract the parameters u_{*t} , α , and C_d from the dust flux data sets. Because u_{*t} is required to determine the other parameters, we first determined the soil's threshold friction velocity for each data set.

Since many field experiments did not report the threshold friction velocity, and because of differences in the definition of threshold between data sets that did report a threshold friction velocity, we estimated u_{*t} in a similar manner for each data set as described in detail in Appendix B in the Supplement. In brief, we estimated u_{*t} using least-squares fitting of a second order Taylor series of Eq. (23) below to saltation flux measurements within a limited range around the threshold (Barchyn and Hugenholtz, 2011). If the data set did not contain sand flux measurements, we instead used a least-squares fit of a second order Taylor series of Eq. (19) to measurements of the dust flux.

After determining u_{*t} in this manner, we use the following procedure to extract C_d and α from each data set's dust flux measurements. Following Eq. (7), we start by calculating the dimensionless dust flux for each measurement of F_d at given values of u_* and u_{*t} (obtained as described below) as

$$\tilde{F}_d = \frac{F_d}{f_{\text{bare}} f_{\text{clay}} \rho_a (u_*^2 - u_{*t}^2) / u_{*st}}. \quad (21)$$

Through substitution of Eq. (19) we now obtain an analytical expression for \tilde{F}_d as a function of C_d and α ,

$$\tilde{F}_d = C_d \left(\frac{u_*}{u_{*t}} \right)^\alpha. \quad (22)$$

We then use least-squares fitting of Eq. (22) to the values of \tilde{F}_d calculated from dust flux measurements to determine the dust emission coefficient C_d and the fragmenta-

Title Page

Abstract

Introduction

Conclusions

References

Tables

Figures

◀

▶

◀

▶

Back

Close

Full Screen / Esc

Printer-friendly Version

Interactive Discussion



tion exponent α , as well as their uncertainties, for each data set. The least-squares fitting procedure and the calculation of uncertainties is described in more detail in the Supplement.

In addition, we obtain an independent estimate of the fragmentation exponent α , and thus the dust emission exponent $a = \alpha + 2$, by using measurements of the *sandblasting efficiency*, which is defined as the ratio of the vertical dust flux to the horizontal saltation flux (Gillette, 1979). The sandblasting efficiency is thus defined for the data sets that reported measurements of both the dust flux and the (impact) flux of saltators at a certain height (i.e., ZP06, SA09, and SI11). This latter variable was usually measured with the Sensit piezoelectric instrument (Stockton and Gillette, 1990), which has been shown provide a good measure of the horizontal saltation flux (Gillette et al., 1997; van Donk et al., 2003).

We extract α from measurements of the sandblasting efficiency as follows. We start with the saltation mass flux, which is given by (Bagnold, 1941; Kok et al., 2012)

$$Q = \rho_a \left(u_*^2 - u_{*t}^2 \right) \frac{L}{\Delta v}, \quad (23)$$

where L is the typical saltation hop length, and Δv is the average difference between saltators' impact and lift-off speeds. The ratio $L/\Delta v$ is thought to scale with the friction velocity,

$$\frac{L}{\Delta v} \propto u_*^r, \quad (24)$$

where the exponent r ranges from 0 (Ungar and Haff, 1987; Duran et al., 2011; Ho et al., 2011; Kok et al., 2012) to 1 (Owen, 1964; Shao et al., 1993), such that we take $r = 0.5 \pm 0.5$. We now obtain an analytical expression for the sandblasting efficiency by combining Eqs. (19), (23) and (24)

$$\frac{F_d}{Q} = C_s u_*^{\alpha-r}, \quad (25)$$

An improved dust emission model

J. F. Kok et al.

| | |
|--------------------------|--------------|
| Title Page | |
| Abstract | Introduction |
| Conclusions | References |
| Tables | Figures |
| ◀ | ▶ |
| ◀ | ▶ |
| Back | Close |
| Full Screen / Esc | |
| Printer-friendly Version | |
| Interactive Discussion | |



An improved dust emission model

J. F. Kok et al.

Title Page

Abstract

Introduction

Conclusions

References

Tables

Figures

I◀

▶I

◀

▶

Back

Close

Full Screen / Esc

Printer-friendly Version

Interactive Discussion



where the dimensional constant C_s contains all parameters that do not depend on u_* . We then obtain α and its uncertainty by fitting measurements of the sandblasting efficiency to the power law in u_* of Eq. (25); this procedure is described in more detail in the Supplement. Note that an important advantage of the calculation of α from the sandblasting efficiency is that, unlike the calculation of α from the dimensionless dust flux described above, the result does not depend on the determination of the threshold friction velocity u_{*t} . Therefore, errors that arise due to the procedure for assessing u_{*t} do not affect the estimate of α derived from the sandblasting efficiency.

3.4 Test of parameterization's functional form with dust flux measurements

All 11 data sets from the six studies that met the quality-control criteria discussed in Sect. 3.1 were used to determine the fragmentation exponent α through non-linear least-squares fitting of Eq. (22) to the vertical dust flux (see Supplement Fig. S4). Furthermore, five data sets featured simultaneous dust flux and saltation flux measurements, which we used to determine α by fitting Eq. (18) to the ratio of the vertical dust and horizontal saltation (impact) fluxes (see Supplement Fig. S5), and seven data sets were taken over spatially homogeneous terrain and thus were used to determine the dust emission coefficient C_d (see Supplement Fig. S4).

The resulting analysis of the compilation of quality-controlled dust flux data sets shows an approximately linear increase in the dust emission exponent α with u_{*st} (Fig. 4a), as predicted by Eq. (17). We obtain the dimensionless constant C_α using least-squares fitting of Eq. (17), yielding $C_\alpha = 2.7 \pm 1.0$. Moreover, the literature-extracted data sets show an approximately exponential decrease of the dust emission coefficient C_d with u_{*st} , as also predicted from our theory (Eq. 19) and numerical simulations (Fig. 4b). We obtain $C_e = 2.0 \pm 0.3$ and $C_{d0} = (4.4 \pm 0.5) \times 10^{-5}$ from least squares fitting of Eq. (19b).

3.5 Test of parameterization's predictions with dust flux measurements

After testing the parameterization's functional form and determining the values of its coefficients, we can compare the predictions of Eq. (19) with measurements of F_d (Fig. 5). For reference, we also compare against the predictions of the existing parameterizations GP88 (Gillette and Passi, 1988) and MB95 (Marticorena and Bergametti, 1995). These parameterizations are respectively given by

$$F_d = C_{GP} f_{bare} u_*^4 (1 - u_{*t}/u_*), \quad (26)$$

and

$$F_d = C_{MB} \eta f_{bare} \frac{\rho_a}{g} u_*^3 \left(1 - \frac{u_{*t}^2}{u_*^2}\right) \left(1 + \frac{u_{*t}}{u_*}\right), \quad (27)$$

where Eq. (27) simplifies Eq. (34) in Marticorena and Bergametti (1995) by using a single value of u_{*t} for the soil rather than different thresholds for different soil particle size bins, which is a common simplification (e.g., Zender et al., 2003a) and supported by measurements (Kok et al., 2012). The parameters C_{GP} ($\text{kg m}^{-6} \text{s}^3$) and C_{MB} (dimensionless) are proportionality constants, and the sandblasting efficiency η depends on the clay fraction following $\eta = 10^{13.4f_{clay}-6}$. Note that we unfortunately cannot compare our measurements compilation against the physically-explicit dust flux parameterizations of Shao and colleagues (Shao et al., 1993, 1996; Shao, 2001), because these parameterizations use detailed soil properties that are unavailable for most data sets.

Our proposed parameterization reproduces measurements with over a factor of two less error than these existing parameterizations (Fig. 5a–c and Table 2). Eq. (19) also produces better agreement when each parameterization's proportionality constant is tuned to each individual data set (Supplement Fig. S2 and Table 2). However, due to the scarcity of quality vertical dust flux measurements, the same measurements used to determine the dimensionless parameters C_α , C_e , and C_{d0} (Fig. 4) were used to test

Title Page

Abstract

Introduction

Conclusions

References

Tables

Figures

◀

▶

◀

▶

Back

Close

Full Screen / Esc

Printer-friendly Version

Interactive Discussion



An improved dust emission model

J. F. Kok et al.

Title Page

Abstract

Introduction

Conclusions

References

Tables

Figures

◀

▶

◀

▶

Back

Close

Full Screen / Esc

Printer-friendly Version

Interactive Discussion



the theory's predicted dust flux. Therefore, the comparison between the parameterizations given in Figs. 5a-c is not on a fully equal footing. We have thus also included comparison graphs for which the coefficients in each parameterization are tuned to produce maximum agreement within the physically plausible parameter range. That is, we tuned the parameters for each parameterizations so as to minimize the sum of the average root mean square error for each dataset (i.e., each dataset is weighted equally, irrespective of how many data points it contains).

The tuned coefficients include the u_* exponent, which is 4 in Gillette and Passi (1988) and 3 in Marticorena and Bergametti (1995). Physically, this exponent cannot be smaller than 2, since the wind stress scales with u_*^2 (Bagnold, 1941; Kok et al., 2012; Shao, 2008). Interestingly, for both parameterizations, the agreement with the vertical dust flux parameterization is maximized when the exponent is tuned to this minimum value of 2. For the MB95 parameterization, we also tuned the coefficient scaling the dependence of the dust flux on the clay fraction, which is 13.4 in the original study. Restricting this parameter to the physically realistic range of greater than or equal to zero (i.e., the dust flux increases with clay fraction, as observed (Gillette, 1979; Sweeney and Mason, 2013) and argued here and in Marticorena and Bergametti, 1995), we found that, surprisingly, best agreement with measurements occurs when we take this parameter equal to zero. Finally, we tuned the proportionality constants in both parameterizations, which yielded $C_{\text{GP}} = 1.05 \times 10^{-5} \text{ kg m}^{-4} \text{ s}$ and $C_{\text{MB}} = 29.5$. For consistency, we also tuned the parameters in Eq. (19), which yielded values close to those obtained by the fitting process in Figs. 3a and 3b, namely $C_{\text{d0}} = 6.17 \times 10^{-5}$, $C_e = 2.0$, and $C_a = 1.7$. Figure 4d-f and Table 2 show that tuning the parameters in the empirical parameterizations substantially improves their agreement against the measurement compilation, yet the agreement of Eq. (19) with measurements is even better.

3.6 Limitations of the dust emission theory and parameterization

We derived the dust emission parameterization of Eq. (19) for dust emission occurring primarily through the fragmentation of soil aggregates of dust particles by impacting

An improved dust emission model

J. F. Kok et al.

Title Page

Abstract

Introduction

Conclusions

References

Tables

Figures

◀

▶

◀

▶

Back

Close

Full Screen / Esc

Printer-friendly Version

Interactive Discussion



saltators. Nonetheless, the main assumption used in deriving Eq. (19) is the existence of a normally-distributed threshold controlling dust emission. Consequently, Eq. (19) theoretically applies to any dust emission processes controlled by an approximately normally-distributed threshold. This point is underscored by the insensitivity of the functional form of Eqs. (17) and (18) to the threshold's normal distribution parameters and the saltator size (Fig. 2). Examples of dust emission processes other than fragmentation that are controlled by a normally-distributed threshold could include dust emission from crusted soils (Rice et al., 1996) and from sand particles with clay coatings (Bullard et al., 2004). Since we do not know what the relative contribution of different dust emission processes is to each of the dust flux data sets used to calibrate the dimensionless coefficients in Eq. (19), it is likely that the obtained values of these coefficients represents some weighted average of the relative contribution of each dust emission process. As discussed in Sect. 2.2, we consider it most likely that the fragmentation process contributes the largest fraction of the dust flux for each data set. Thus, although our parameterization theoretically applies to dust emission from soils dominated by processes other than fragmentation, the dimensionless coefficients in Eq. (19) could be quite different for such soils. We are not aware of any experimental data sets that meet our quality-control criteria that could be used to estimate the dimensionless coefficients for soils for which dust emission is dominated by any specific process other than fragmentation.

Furthermore, as mentioned in Sect. 2.2.1, our theory applies only to soils for which the saltation flux is limited by the availability of wind momentum, and are thus *transport limited* (e.g., Nickling and McKenna Neuman, 2009). The present theory is thus not valid for soils for which the horizontal saltation flux at a given point in time is limited by the availability of sand-sized sediment. Such *supply-limited* soils are inherently inefficient sources of dust aerosols (Rice et al., 1996), and are thus probably less important in the global dust budget. Note that dust emission from some prominent sources can be limited by the sediments supplied to these sources, for instance through the deposition of fluvially-eroded sediment (Bullard et al., 2011; Ginoux et al., 2012). However,

when substantial emission occurs from such regions, the soil is generally not supply limited at that point in time (Bullard et al., 2011), such that Eq. (19) could be used to parameterize the dust flux.

Our parameterization attempts to include only the most important processes affecting the dust flux. Eq. (19) thus does not explicitly account for many other processes that might affect dust emission, including changes in the parameters γ and ε with u_* and u_{*t} , and the dependence of c_ψ and σ_ψ on the soil size distribution, mineralogy, and other soil properties. Future studies should consider these effects, especially if more extensive global (or regional) soil data sets become available, or if more dust flux data sets that sufficiently characterize these soil properties become available. However, as mentioned above, many of these processes partially affect the dust emission flux F_d by increasing or decreasing u_{*st} , such that some of their effect might be captured in the calibration of the dimensionless coefficients of Eq. (19) to our compilation of vertical dust flux data sets.

Another limitation of our theory is that it does not account for dust emission due to saltator impacts that do not produce fragmentation but that nonetheless produce dust by “damaging” the dust aggregate (Kun and Herrmann, 1999). It also does not account for the lowering of an aggregate’s fragmentation threshold through the rupturing of cohesive bonds by impacting saltators. These effects might dominate for very erosion-resistant soils, such as crusted soils. A further limitation of our theory is that it simplifies the energetics of dust emission by considering u_{*st} the prime determinant of soil erodibility (Shao and Lu, 2000). Although the threshold for saltation (u_{*st}) and the threshold energy required to fragment dust aggregates (ψ) are likely strongly coupled for many soils (Shao et al., 1993; Rice et al., 1996; Rice et al., 1999), increases in ψ might not produce corresponding increases in u_{*st} for some soils. An example of such a soil is a sandy soil for which dust emissions occurs primarily from the removal of dust coatings on sand grains (Bullard et al., 2004), and emission from such soils might thus be poorly captured by the present theory.

An improved dust emission model

J. F. Kok et al.

Title Page

Abstract

Introduction

Conclusions

References

Tables

Figures

◀

▶

◀

▶

Back

Close

Full Screen / Esc

Printer-friendly Version

Interactive Discussion



4 Assessment of parameterization performance in a climate model

It is encouraging that the functional form of Eq. (19) is consistent with measurements (Fig. 4), and that Eq. (19) also better captures variability in dust flux measurements than previous parameterizations (Fig. 5 and Table 2). Another critical test of our scheme is whether it actually improves the representation of the global dust cycle in climate models. As discussed in the Introduction, the fact that source functions, which tend to shift dust emissions towards regions with high observed dust loadings, improve model agreement with observations (e.g., Cakmur et al., 2006) suggests a gap in climate model representation of dust emission physics. And indeed, accounting for our finding that the dust flux is more sensitive to soil erodibility (see Sect. 2.3) would shift dust emissions towards the most erodible regions, possibly producing an effect similar to that of applying a source function. This suggests that our new parameterization might (partially) eliminate the need for an empirical source function in dust cycle simulations.

We used simulations with the Community Earth System Model (CESM) version 1.1 to both test the above hypothesis, and to assess our parameterization's performance against measurements from the AERosol Robotic NETwork (AERONET), which are thus independent from those used to test our theory in Fig. 5. Specifically, we simulated the present-day dust cycle with four different combinations of source functions and dust flux parameterizations (see Table 3). We then tested the ability of each model configuration to reproduce the present-day dust cycle by quantitatively comparing the simulated aerosol optical depth (AOD) against AERONET measurements.

In the next section, we briefly describe the CESM model, its treatment of the dust cycle, and our methods for comparing the simulation results against AERONET measurements. We then present the results of the simulations, and their quantitative comparison against AERONET measurements, in Sect. 4.2.

Title Page

Abstract

Introduction

Conclusions

References

Tables

Figures

◀

▶

◀

▶

Back

Close

Full Screen / Esc

Printer-friendly Version

Interactive Discussion



4.1 CESM model setup

Emission of dust aerosols was calculated with CESM's land model, the Community Land Model version 4.0 (CLM4, Lawrence et al., 2011). These emissions were then used by CESM's atmosphere model, the Community Atmosphere Model version 4 (CAM4), to calculate the dust optical depth, as well as the transport and deposition of dust (Mahowald et al., 2006b).

In addition to accounting for the global dust cycle and the consequent optical depth produced by dust aerosols (see next section), CESM also accounts for the effects of other kinds of aerosols, such as sea salt, biomass burning, and sulfate aerosols. Black and organic carbon, dimethyl-sulphide, and sulphur oxides emissions are prescribed based on AEROCOM specifications (Neale et al., 2010), whereas sea salt aerosol emission is prognostic, based on 10 m wind speed and humidity (Mahowald et al., 2006a).

4.1.1 Treatment of the dust cycle in CESM

The emission of dust aerosols in CLM4 follows the treatment of Zender et al. (2003a), with modifications described in Mahowald et al. (2006b, 2010). Specifically, the vertical dust flux ϕ_d in a model grid cell is parameterized using Eq. (1), with the vertical dust flux F_d and the source function S given in Table 3 for the four simulations. The global tuning factor C_{tune} is adjusted to maximize agreement against AERONET measurements, as described in more detail in Sect. 4.1.2.

The main determinant of u_{*st} in CLM4 is the soil moisture content. CLM4 follows Zender et al. (2003a) in parameterizing the effect of soil moisture on the dust emission

Title Page

Abstract

Introduction

Conclusions

References

Tables

Figures

◀

▶

◀

▶

Back

Close

Full Screen / Esc

Printer-friendly Version

Interactive Discussion



threshold u_{*t} following Eqs. (12) and (14) in Fécan et al. (1999). That is,

$$\frac{u_{*t}}{u_{*dt}} = 1, \quad (w < w') \quad (28)$$

$$\frac{u_{*t}}{u_{*dt}} = \sqrt{1 + 1.21(w - w')^{0.68}} \quad (w \geq w'), \quad (29)$$

5 where u_{*t} and u_{*dt} are the dust emission thresholds in the presence and absence of soil moisture, respectively, and w is the gravimetric water content in percent for the model's top soil layer, which has a thickness of 1.75 cm (Oleson et al., 2010). The threshold gravimetric water content w' of the top soil layer above which w increases u_{*t} is given by (Fecan et al., 1999; Zender et al., 2003a)

$$10 \quad w' = b \left(0.17\rho_{\text{clay}} + 0.0014\rho_{\text{clay}}^2 \right), \quad (30)$$

where w' is given in percent, and $\rho_{\text{clay}} = 100f_{\text{clay}}$ is the soil's clay content in percent. The tuning parameter b was introduced by Zender et al. (2003a), and the range of plausible values extends from 1 (i.e., no tuning constant; Fecan et al., 1999) to 3 (Mokhtari et al., 2012) to $1/f_{\text{clay}}$ (Zender et al., 2003a). The larger the value of b , the smaller the effect of soil moisture on the dust emission threshold u_{*t} . Since dust emissions are non-linear in u_{*t} , and since u_{*t} is a critical variable in our parameterization, the choice of b can be expected to substantially affect the simulated dust cycle. Furthermore, the parameterization of Fecan et al. (1999) is largely based on wind tunnel studies, such that implementing this small-scale parameterization into a GCM scales it up by many orders of magnitude, potentially producing physically unrealistic results. Furthermore, the inhibition of dust emission by soil moisture depends on the moisture content of the very top layer of soil particles (McKenna Neuman and Nickling, 1989), which is in direct contact with the surface air. In contrast, the top soil layer of hydrology models in climate models usually has a thickness of multiple centimeters and thus responds differently to precipitation and changes in atmospheric humidity, which are important in

An improved dust emission model

J. F. Kok et al.

Title Page

Abstract

Introduction

Conclusions

References

Tables

Figures

◀

▶

◀

▶

Back

Close

Full Screen / Esc

Printer-friendly Version

Interactive Discussion



An improved dust emission model

J. F. Kok et al.

Title Page

Abstract

Introduction

Conclusions

References

Tables

Figures

◀

▶

◀

▶

Back

Close

Full Screen / Esc

Printer-friendly Version

Interactive Discussion



determining the dust emission threshold (Ravi et al., 2004, 2006). Consequently, the “correct” value of b in a climate model is likely to depend substantially on the model methodology, and in particular on the model treatment of hydrology. Since the choice of b is thus ambiguous, we investigated the sensitivity of our results to the particular value of b by running simulations with a wide range of values (Table 4). Because we found that the simplest case of not using a tuning constant (i.e., $b = 1$) produces the best results for all four model configurations (see Tables 3 and 4), we used $b = 1$ for the results reported in Sect. 4.2. But note that the wide range of values of b that we tested all produced qualitatively similar results to those presented in Sect. 4.2 (see Table 4).

In addition to the effects of soil moisture, CLM4 also accounts for the inhibition of dust emissions by vegetation. Specifically, CLM4 assumes that the fraction of the grid cell consisting of bare soil capable of emitting dust aerosols decreases linearly with the leaf area index (LAI), which denotes the ratio of the total surface area of leafs with the land surface area. That is,

$$f_{\text{bare}} = 1 - \lambda / \lambda_{\text{thr}}, \quad (\lambda \leq \lambda_{\text{thr}}) \quad (31)$$

where λ denotes LAI, and $\lambda_{\text{thr}} = 0.3$ is the threshold LAI above which no dust emission occurs (Mahowald et al., 2010). (Note that the Ginoux et al., 2001 source function already includes the effects of vegetation, such that $f_{\text{bare}} = 1$ for all grid cells for Simulation III (see Table 4)).

CESM distributes the emitted dust aerosols into 4 size bins (Mahowald et al., 2006b), from 0.1–1.0 μm , 1.0–2.5 μm , 2.5–5.0 μm , and 5.0–10 μm , following Eq. (7) in Kok (2011b). The optical properties for each bin (Albani et al., 2013) are derived from a representation of dust as an internal mixture of the primary mineral classes of dust (quartz, aluminosilicates, clays, carbonates, iron-bearing minerals), combined into an effective medium using the Maxwell Garnett approximation (e.g., Videen and Chylek, 1998). The proportions of the mineral classes are consistent with the ranges reported in atmospheric dust and its parent soils (Claquin et al., 1999), and are in agreement with

bulk optical properties observed in dusty regions (Albani et al., 2013). The radiative effects of dust aerosols do not feed back onto the atmospheric dynamics.

CAM4 simulates both dry and wet deposition of dust. Dry deposition includes turbulent and gravitational settling, and follows the treatment in Zender et al. (2003a).

Wet deposition accounts for in- and below-cloud scavenging, and follows Neale et al. (2010), with the modifications described in Albani et al. (2013), which improve the model's ability to simulate the observed spatial gradients of dust. Specifically, the dust solubility (i.e., the fraction of dust available for in-cloud removal) was changed from 0.15 to 0.30, in line with a more recent version of the model (Liu et al., 2012).

In addition, instead of using a constant below-cloud scavenging coefficient (collection efficiency) of 0.1 (Balkanski et al., 1993; Neale et al., 2010), the scavenging coefficient was made size-dependent (Andronache, 2003; Zender et al., 2003a), and was set to 0.1 for dust diameters below 2.5 μm and 0.3 for larger dust particles.

4.1.2 Quantitative comparison of CESM simulations against AERONET AOD data

We quantify the ability of each simulation to reproduce the global dust cycle by comparing the simulated AOD against the extensive and accurate measurements of the AERONET network (Eck et al., 1999; Holben et al., 1998). AERONET sites contain measurements from sun photometers of radiances at many wavelengths, which are then inverted to retrieve aerosol properties (Dubovik et al., 2002). We select stations for which our simulations indicate that over 50 % of the annually-averaged AOD is due to dust aerosols (i.e., stations which lie on or within the 50 % dust AOD boundary for 3 or more of the 4 simulations in Supplement Fig. S6i–l). Furthermore, for each station, we select only days for which the Angstrom exponent AE (in the 440–870 nm wavelength range) is smaller than 1 (Dubovik et al., 2002; Eck et al., 1999). Since AE is a measure of particle size, with smaller values indicating coarser aerosols, values of $AE < 1$ indicate that a substantial fraction of AOD is due to dust (Dubovik et al., 2002; Eck et al., 1999). Choosing a different plausible cut-off for AE does not qualitatively

An improved dust emission model

J. F. Kok et al.

Title Page

Abstract

Introduction

Conclusions

References

Tables

Figures

◀

▶

◀

▶

Back

Close

Full Screen / Esc

Printer-friendly Version

Interactive Discussion



affect our results. Finally, we select only stations for which at least 6 months of data (i.e., 183 days) is available over the simulation period.

The above procedure resulted in the selection of 40 stations: 17 in North Africa, 4 in the North Atlantic, 10 in the Middle East, 6 in the rest of Asia, and 3 in Australia (Figs. 6–8). For each station, we averaged the AOD over all days with a substantial dust contribution (as determined from the value of AE, see above) and then calculated the modeled AOD for each simulation, averaged over those same days. The resulting comparison between simulated and measured average AOD at these stations (Fig. 7) is sensitive to the value of the parameter C_{tune} (see Eq. 1), which scales the size of the global dust cycle. Because of the many uncertainties in parameterizing dust emission on both small scales (Fig. 5) and the much larger model grid box scale, the value of C_{tune} is poorly constrained (Cakmur et al., 2006; Huneus et al., 2011). We therefore adjust the value of C_{tune} for each of the four simulations in order to minimize the root mean square error (RMSE) against the AERONET AOD measurements of Fig. 7. That is, we determine C_{tune} by minimizing:

$$\text{RMSE} = \frac{1}{N} \sqrt{\sum_i^N (\tau_{\text{model},i} - \tau_{\text{meas},i})^2} \quad (32)$$

where i sums over the $N = 40$ AERONET stations and τ_{model} is the AOD in the visible wavelength simulated at the AERONET station location, the component of which that is due to dust aerosols scales with C_{tune} . The measured AERONET AOD (τ_{meas}) is obtained at 550 nm, the central wavelength in the visible spectrum, by correcting the AOD measured at 675 nm to 550 nm using the measured value of the Angstrom exponent α . That is,

$$\tau_{\text{meas},i} = \tau_{675,i} \left(\frac{\lambda_{675}}{\lambda_{550}} \right)^\alpha \quad (33)$$

where τ_{675} is the measured AOD at 675 nm, and λ_{550} and λ_{675} equal 550 and 675 nm, respectively.

An improved dust emission model

J. F. Kok et al.

Title Page

Abstract

Introduction

Conclusions

References

Tables

Figures

◀

▶

◀

▶

Back

Close

Full Screen / Esc

Printer-friendly Version

Interactive Discussion



4.2 CESM simulation results and quantitative comparison against AERONET AOD

We used CESM to run four different simulations. The “control” Simulation I uses CESM’s default parameterization (MB95) and does not use a source function; Simulations II and III then respectively add the source functions of Zender et al. (2003b) and Ginoux et al. (2001); and Simulation IV replaces the MB95 parameterization with Eq. (19) and also does not use a source function (see Table 3). For these simulations, we used the capability of CESM to be forced with reanalysis winds instead of predicting winds, and used the reanalysis meteorology from the European Centre for Medium-range Weather Forecasts (ECMWF) (Dee et al., 2011; Ma et al., 2013) from 2000 to 2011. The first year of each simulation was used as model spin-up and thus not used for analysis. All simulations were run at a resolution of 1.9° latitude by 2.5° longitude.

Results of the four simulations are shown in Figs. 6 and 7, which show global maps of respectively the vertical dust flux and the resulting dust AOD. Supplement Fig. S6 further shows global maps for each simulation of the dust AOD, the AOD produced by all aerosols, and the fraction of the simulated aerosol optical depth that is due to dust. It can be seen that application of a source function tends to shift dust emissions and dust AOD from less erodible regions, such as North America, to more erodible regions, such as North Africa (Figs. 6b, c, 7b, and c). As hypothesized above, replacing MB95 with Eq. (19) shifts dust AOD to more erodible regions in a manner that appears qualitatively similar to applying a source function, particularly to that of applying the Ginoux et al. (2001) source function (compare Fig. 7c and d). That is, it produces increases in emissions and AOD over most of North Africa and decreases over less erodible regions such as North America and Southern Africa (Figs. 6d and 7d). Moreover, the new parameterization shifts dust AOD within North Africa southward towards the 15–25° latitude belt, bringing the simulations in better qualitative agreement with satellite observations (Ashpole and Washington, 2013; Ginoux et al., 2012; Prospero et al.,

An improved dust emission model

J. F. Kok et al.

Title Page

Abstract

Introduction

Conclusions

References

Tables

Figures

◀

▶

◀

▶

Back

Close

Full Screen / Esc

Printer-friendly Version

Interactive Discussion



2002; Schepanski et al., 2009). Furthermore, the new parameterization predicts substantial increases in dust emission in Patagonia (Figs. 6d and 7d), which in the default version of CESM needs to be increased by about two orders of magnitude to match available observations (Albani et al., 2013).

5 The global maps of dust AOD in Fig. 6 thus suggest that our more physically-based scheme better captures the relative contributions of the different source regions to the global dust loading. This is confirmed by the quantitative comparisons between the simulated AOD and that measured at AERONET stations (Fig. 8). As expected, the application of the source functions of both Zender et al. (2003b) and Ginoux et al. (2001) improve agreement with AERONET data (Fig. 8a–c). However, substantially better agreement is obtained with Simulation IV, which uses Eq. (19) and does not use a source function. In particular, Simulation IV produces improved agreement over North Africa, the Middle East, and Australia, and somewhat lesser agreement over Asia.

5 Discussion

15 Our dust flux parameterization includes two main improvements over previous schemes (Gillette and Passi, 1988; Marticorena and Bergametti, 1995). First, it accounts for the predicted (Figs. 1 and 2a) and observed (Fig. 4a) increasing scaling of F_d with u_* that occurs with increasing u_{*st} ; this advance helps explain the numerous observed scalings of F_d with u_* (Kok et al., 2012; Shao, 2008). Second, our parameterization accounts for a soil's reduced ability to produce dust under saltation bombardment as u_{*st} increases (Figs. 1, 2b, and 4b).

This second improvement is especially important, as it implies that previous parameterizations have underestimated the sensitivity of the dust flux to u_{*st} , and thus to soil erodibility (Fig. 9). This underestimation is not sensitive to the details of our parameterization because it follows directly from the energetics of dust emission: increases in soil cohesion both raise the threshold and cause dust emission to require more energy, thereby reducing the dust flux for a given saltator kinetic impact energy. This effect was

Title Page

Abstract

Introduction

Conclusions

References

Tables

Figures

◀

▶

◀

▶

Back

Close

Full Screen / Esc

Printer-friendly Version

Interactive Discussion



previously noted by Shao and colleagues (Shao, 2001; Shao et al., 1996), yet not included in dust emission parameterizations commonly implemented in climate models (e.g., Ginoux et al., 2001; Zender et al., 2003a; Cakmur et al., 2006).

The simulation of the dust cycle with our new parameterization, which accounts for the dust flux's increased sensitivity to soil erodibility, shows a shift in emissions and dust AOD to highly erodible regions such as North Africa (Fig. 7d). This effect is qualitatively similar to that of applying a source function (see especially Fig. 7c). Simulations with our new parameterization are also in better agreement with AERONET data than simulations using a source function (Fig. 8b–d). These results suggest that part of the sensitivity of the dust flux to soil erodibility in present models is accounted for by the source function. Consequently, our new parameterization reduces, or possibly eliminates, the need for a source function. This needs to be further investigated with other models and more data sets, including data sets of deposition (Kohfeld and Harrison, 2001) and surface concentration (Prospero and Nees, 1986).

Our result that the dust flux is more sensitive to the soil erodibility than most current models account for emphasizes the importance of accurately represent spatial and temporal variations in soil erodibility. Our parameterization provides a convenient way of accounting for this through variations in the standardized dust emission threshold u_{*st} . However, the parameterization of u_{*st} in most models is relatively primitive (e.g., Zender et al., 2003a). For instance, one of the main determinants of u_{*st} is the moisture content of the topsoil, yet the most commonly-used parameterization of the effect of soil moisture on u_{*st} (Fecan et al., 1999) is found to produce unrealistic results in some models, requiring the use of a tuning constant (Mokhtari et al., 2012; Zender et al., 2003a). Furthermore, effects of soil aggregation and crust formation on u_{*t} are generally not included in the leading global dust modules (Ginoux et al., 2001; Zender et al., 2003a). Considering the paramount importance of u_{*st} in determining dust fluxes (see Eq. 19), an effective way to further improve the fidelity of global dust cycle simulations would thus be to develop improved parameterizations that describe u_{*st} as a function of soil properties, precipitation events, atmospheric relative humidity, and

An improved dust emission model

J. F. Kok et al.

Title Page

Abstract

Introduction

Conclusions

References

Tables

Figures

◀

▶

◀

▶

Back

Close

Full Screen / Esc

Printer-friendly Version

Interactive Discussion



An improved dust emission model

J. F. Kok et al.

Title Page

Abstract

Introduction

Conclusions

References

Tables

Figures

◀

▶

◀

▶

Back

Close

Full Screen / Esc

Printer-friendly Version

Interactive Discussion



other relevant parameters. Alternatively, for simulations of the current dust cycle, u_{*st} could in principle be remotely sensed (Chomette et al., 1999; Draxler et al., 2010). Doing so requires the simultaneous determination of the threshold wind speed and the surface roughness (Marticorena et al., 2004), such that the remotely-sensed threshold wind stress can be partitioned between the portion causing dust emission (τ_S) and that absorbed by non-erodible elements (τ_R) (Marticorena and Bergametti, 1995; Raupach et al., 1993).

The underestimation of the dust flux's sensitivity to soil erodibility by climate models also has important implications for evaluating the global dust cycle in a changing climate. In particular, since soil erodibility is affected by climate, which partially determines the soil moisture content, aggregation state, and crusting of the soil (Kok et al., 2012; Zobeck, 1991), our results suggest that climate models have underestimated the dust cycle's climate sensitivity. This result could help explain a series of observations. For instance, models have difficulty reproducing the increase in North African dust emissions during the Sahel drought in the 1980s (Mahowald et al., 2002), which is likely due, in part, to the underestimation of the dust flux's sensitivity to drought conditions (Fig. 9). Furthermore, an increased sensitivity of dust emissions to climate could help explain the large differences in the global dust cycle between different climates, such as large increases in dust deposition during the Last Glacial Maximum (Rea, 1994; Harrison et al., 2001), which climate models also have difficulty reproducing without positing large changes in source areas (Werner et al., 2002; Mahowald et al., 2006b).

6 Summary and conclusions

We have used a combination of theory and numerical simulations to derive a physically-based parameterization of the vertical dust flux emitted by an eroding soil. The resulting dust emission scheme uses only parameters that are readily available in regional and global climate models and is straightforward to implement. Our new parameterization

An improved dust emission model

J. F. Kok et al.

Title Page

Abstract

Introduction

Conclusions

References

Tables

Figures

◀

▶

◀

▶

Back

Close

Full Screen / Esc

Printer-friendly Version

Interactive Discussion



accounts for two processes that were not included in previous schemes used in climate models: (i) the increasing scaling of dust flux with wind speed that occurs as a soil becomes less erodible and only the most energetic saltators become capable of producing dust (Figs. 2a and 4a), and (ii) the soil's reduced ability to produce dust under saltation bombardment as it becomes less erodible (Figs. 2b and 4b). The treatment of both these processes in our dust emission model is supported by a quality-controlled compilation of field measurements (Fig. 4). Partially as a result of the inclusion of these additional physical processes, our parameterization is in better agreement with dust flux measurements than previous schemes used in climate models (Fig. 5).

An important insight from our dust emission scheme is that current parameterizations in climate models likely underestimate the dust flux's sensitivity to the soil erodibility (Fig. 9). In fact, our results indicate that current models (partially) account for the missing component of the dust flux's sensitivity to soil erodibility through the use of empirical preferential sources functions (e.g., Ginoux et al., 2001). Since the parameterization presented here does account for this missing component, it seems to eliminate the need to use a source function to reproduce the dust cycle in climate models (compare Fig. 7c and d). Indeed, CESM model simulations show that the new parameterization produces agreement with AERONET AOD measurements that is even better than that obtained by using a source function (Fig. 8).

Accounting for the dust flux's increased sensitivity to soil erodibility will affect simulations of the global dust cycle's response to future climate changes. In particular, since arid regions are predicted to become drier in most climate models (Solomon et al., 2007), accounting for the increased sensitivity to soil erodibility would likely produce an increase in the future dust flux, and thus dust radiative forcing, relative to simulations that do not account for this. Since the dust cycle is sensitive to a variety of processes, including CO₂ fertilization (Mahowald et al., 2006b), land use change (Ginoux et al., 2012), and changes in sediment availability (Harrison et al., 2001), a substantial body of further work is required to assess the dust cycle's response to future climate changes.

Supplementary material related to this article is available online at
[http://www.atmos-chem-phys-discuss.net/14/6361/2014/
acpd-14-6361-2014-supplement.pdf](http://www.atmos-chem-phys-discuss.net/14/6361/2014/acpd-14-6361-2014-supplement.pdf).

Acknowledgements. We thank Stéphane Alfaro, Jean Louis Rajot, and Béatrice Marticorena for providing the measurements of Sow et al. (2009), and for providing comments that helped improve the manuscript. Comments by Shanna Shaked also helped improve the manuscript. We also thank the AERONET principal investigators and their staff for establishing and maintaining the 40 sites used in this investigation. This work was supported by the National Science Foundation (NSF) under grant numbers AGS 0932946 and 1137716. The CESM simulations were conducted at the National Center for Atmospheric Research's Computation Information Systems Laboratory, an NSF-funded facility. Any opinions, findings, and conclusions or recommendations expressed in this material are those of the authors and do not necessarily reflect the views of the National Science Foundation.

References

- Albani, S., Mahowald, N. M., Perry, A. T., Scanza, R. A., Zender, C. S., Heavens, N. G., Maggi, V., Kok, J. F., and Otto-Bliesner, B. L.: Improved dust representation in the Community Atmospheric Model, *J. Adv. Model. Earth Syst.*, in review, 2014.
- Alfaro, S. C. and Gomes, L.: Modeling mineral aerosol production by wind erosion: Emission intensities and aerosol size distributions in source areas, *J. Geophys. Res.*, 106, 18075–18084, 2001.
- Andronache, C.: Estimated variability of below-cloud aerosol removal by rainfall for observed aerosol size distributions, *Atmos. Chem. Phys.*, 3, 131–143, doi:10.5194/acp-3-131-2003, 2003.
- Ashpole, I. and Washington, R.: A new high-resolution central and western Saharan summertime dust source map from automated satellite dust plume tracking, *J. Geophys. Res.-Atmos.*, 118, 6981–6995, 2013.

ACPD

14, 6361–6425, 2014

An improved dust emission model

J. F. Kok et al.

Title Page

Abstract

Introduction

Conclusions

References

Tables

Figures

◀

▶

◀

▶

Back

Close

Full Screen / Esc

Printer-friendly Version

Interactive Discussion



An improved dust emission model

J. F. Kok et al.

Title Page

Abstract

Introduction

Conclusions

References

Tables

Figures

◀

▶

◀

▶

Back

Close

Full Screen / Esc

Printer-friendly Version

Interactive Discussion



Aubinet, M., Chermanne, B., Vandenhoute, M., Longdoz, B., Yernaux, M., and Laitat, E.: Long term carbon dioxide exchange above a mixed forest in the Belgian Ardennes, *Agr. Forest Meteorol.*, 108, 293–315, 2001.

Bagnold, R. A.: *The Physics of Blown Sand and Desert Dunes*, Methuen, New York, 1941.

5 Balkanski, Y. J., Jacob, D. J., Gardner, G. M., Graustein, W. C., and Turekian, K. K.: Transport and residence times of tropospheric aerosols inferred from a global 3-dimensional simulation of Pb-210, *J. Geophys. Res.-Atmos.*, 98, 20573–20586, 1993.

Barchyn, T. E. and Hugenholtz, C. H.: Comparison of four methods to calculate aeolian sediment transport threshold from field data: Implications for transport prediction and discussion of method evolution, *Geomorphology*, 129, 190–203, 2011.

10 Beladjine, D., Ammi, M., Oger, L., and Valance, A.: Collision process between an incident bead and a three-dimensional granular packing, *Phys. Rev. E*, 75, 061305, doi:10.1103/PhysRevE.75.061305, 2007.

Bevington, P. R. and Robinson, D. K.: *Data Reduction and Error Analysis*, McGraw-Hill, New York, 2003.

15 Buckingham, E.: On physically similar systems, illustrations of the use of dimensional equations, *Phys. Rev.*, 4, 345–376, 1914.

Bullard, J. E., McTainsh, G. H., and Pudmenzky, C.: Aeolian abrasion and modes of fine particle production from natural red dune sands: an experimental study, *Sedimentology*, 51, 1103–1125, 2004.

20 Bullard, J. E., Harrison, S. P., Baddock, M. C., Drake, N., Gill, T. E., McTainsh, G., and Sun, Y. B.: Preferential dust sources: a geomorphological classification designed for use in global dust-cycle models, *J. Geophys. Res.-Earth*, 116, F04034, doi:10.1029/2011JF002061, 2011.

25 Cakmur, R. V., Miller, R. L., Perlwitz, J., Geogdzhayev, I. V., Ginoux, P., Koch, D., Kohfeld, K. E., Tegen, I., and Zender, C. S.: Constraining the magnitude of the global dust cycle by minimizing the difference between a model and observations, *J. Geophys. Res.-Atmospheres*, 111, D06207, doi:10.1029/2005JD005791, 2006.

Cartwright, J.: Particle shape factors, *Ann. Occup. Hyg.*, 5, 163–171, 1962.

30 Chomette, O., Legrand, M., and Marticorena, B.: Determination of the wind speed threshold for the emission of desert dust using satellite remote sensing in the thermal infrared, *J. Geophys. Res.-Atmos.*, 104, 31207–31215, 1999.

Claquin, T., Schulz, M., and Balkanski, Y. J.: Modeling the mineralogy of atmospheric dust sources, *J. Geophys. Res.-Atmos.*, 104, 22243–22256, 1999.

An improved dust emission model

J. F. Kok et al.

Title Page

Abstract

Introduction

Conclusions

References

Tables

Figures

◀

▶

◀

▶

Back

Close

Full Screen / Esc

Printer-friendly Version

Interactive Discussion



- Davies, C. N.: Particle-fluid interaction, *J. Aerosol Sci.*, 10, 477–513, 1979.
- Dee, D. P., Uppala, S. M., Simmons, A. J., Berrisford, P., Poli, P., Kobayashi, S., Andrae, U., Balmaseda, M. A., Balsamo, G., Bauer, P., Bechtold, P., Beljaars, A. C. M., van de Berg, L., Bidlot, J., Bormann, N., Delsol, C., Dragani, R., Fuentes, M., Geer, A. J., Haimberger, L., Healy, S. B., Hersbach, H., Holm, E. V., Isaksen, L., Kallberg, P., Kohler, M., Matricardi, M., McNally, A. P., Monge-Sanz, B. M., Morcrette, J. J., Park, B. K., Peubey, C., de Rosnay, P., Tavolato, C., Thepaut, J. N., and Vitart, F.: The ERA-Interim reanalysis: configuration and performance of the data assimilation system, *Q. J. Roy. Meteor. Soc.*, 137, 553–597, 2011.
- Draxler, R. R., Ginoux, P., and Stein, A. F.: An empirically derived emission algorithm for wind-blown dust, *J. Geophys. Res.-Atmos.*, 115, D16212, doi:10.1029/2009JD013167, 2010.
- Dubovik, O., Holben, B., Eck, T. F., Smirnov, A., Kaufman, Y. J., King, M. D., Tanre, D., and Slutsker, I.: Variability of absorption and optical properties of key aerosol types observed in worldwide locations, *J. Atmos. Sci.*, 59, 590–608, 2002.
- Duran, O., Claudin, P., and Andreotti, B.: On aeolian transport: Grain-scale interactions, dynamical mechanisms and scaling laws, *Aeolian Research*, 3, 243–270, 2011.
- Eck, T. F., Holben, B. N., Reid, J. S., Dubovik, O., Smirnov, A., O'Neill, N. T., Slutsker, I., and Kinne, S.: Wavelength dependence of the optical depth of biomass burning, urban, and desert dust aerosols, *J. Geophys. Res.-Atmos.*, 104, 31333–31349, 1999.
- FAO: Harmonized World Soil Database (version 1.2), FAO, Rome, Italy and IIASA, Laxenburg, Austria, 2012.
- Fecan, F., Marticorena, B., and Bergametti, G.: Parametrization of the increase of the aeolian erosion threshold wind friction velocity due to soil moisture for arid and semi-arid areas, *Ann. Geophys.-Atm. Hydr.*, 17, 149–157, 1999.
- Forster, P., Ramaswamy, V., Artaxo, P., Berntsen, T., Betts, R., Fahey, D. W., Haywood, J., Lean, J., Lowe, D. C., Myhre, G., Nganga, J., Prinn, R., Raga, G., Schulz, M., and Dorland, R. V.: Changes in atmospheric constituents and in radiative forcing, in: *Climate Change 2007: The Physical Science Basis*, edited by: Solomon, S., Qin, D., Manning, M., Chen, Z., Marquis, M., Averyt, K. B., Tignor, M., and Miller, H. L., Cambridge University Press, Cambridge, UK and New York, NY, USA, 129–234, 2007.
- Fratini, G., Ciccioli, P., Febo, A., Forgione, A., and Valentini, R.: Size-segregated fluxes of mineral dust from a desert area of northern China by eddy covariance, *Atmos. Chem. Phys.*, 7, 2839–2854, doi:10.5194/acp-7-2839-2007, 2007.

An improved dust emission model

J. F. Kok et al.

Title Page

Abstract

Introduction

Conclusions

References

Tables

Figures

◀

▶

◀

▶

Back

Close

Full Screen / Esc

Printer-friendly Version

Interactive Discussion



- Gillette, D. A.: Environmental factors affecting dust emission by wind erosion, in: Saharan dust, edited by: Morales, C., Wiley, New York, 71–91, 1979.
- Gillette, D. A. and Passi, R.: Modeling dust emission caused by wind erosion, *J. Geophys. Res.-Atmos.*, 93, 14233–14242, 1988.
- 5 Gillette, D. A., Blifford, I. H., and Fryrear, D. W.: Influence of wind velocity on size distributions of aerosols generated by wind erosion of soils, *J. Geophys. Res.*, 79, 4068–4075, 1974.
- Gillette, D. A., Hardebeck, E., and Parker, J.: Large-scale variability of wind erosion mass flux rates at Owens Lake .2. Role of roughness change, particle limitation, change of threshold friction velocity, and the Owen effect, *J. Geophys. Res.-Atmos.*, 102, 25989–25998, 1997.
- 10 Gillies, J. A. and Berkofsky, L.: Eolian suspension above the saltation layer, the concentration profile, *J. Sediment. Res.*, 74, 176–183, 2004.
- Ginoux, P., Chin, M., Tegen, I., Prospero, J. M., Holben, B., Dubovik, O., and Lin, S. J.: Sources and distributions of dust aerosols simulated with the GOCART model, *J. Geophys. Res.*, 106, 20255–20273, 2001.
- 15 Ginoux, P., Prospero, J. M., Gill, T. E., Hsu, N. C., and Zhao, M.: Global-scale attribution of anthropogenic and natural dust sources and their emission rates based on MODIS Deep Blue aerosol products, *Rev. Geophys.*, 50, RG3005, doi:10.1029/2012RG000388, 2012.
- Gomes, L., Rajot, J. L., Alfaro, S. C., and Gaudichet, A.: Validation of a dust production model from measurements performed in semi-arid agricultural areas of Spain and Niger, *Catena*, 52, 257–271, 2003.
- 20 Gordon, M. and McKenna Neuman, C.: A comparison of collisions of saltating grains with loose and consolidated silt surfaces, *J. Geophys. Res.-Earth*, 114, F04015, doi:10.1029/2009JF001330, 2009.
- Goulden, M. L., Munger, J. W., Fan, S. M., Daube, B. C., and Wofsy, S. C.: Measurements of carbon sequestration by long-term eddy covariance: Methods and a critical evaluation of accuracy, *Glob. Change Biol.*, 2, 169–182, 1996.
- 25 Grini, A., Myhre, G., Zender, C. S., and Isaksen, I. S. A.: Model simulations of dust sources and transport in the global atmosphere: Effects of soil erodibility and wind speed variability, *J. Geophys. Res.-Atmos.*, 110, F04015, doi:10.1029/2009JF001330, 2005.
- 30 Harrison, S. P., Kohfeld, K. E., Roelandt, C., and Claquin, T.: The role of dust in climate changes today, at the last glacial maximum and in the future, *Earth-Sci. Rev.*, 54, 43–80, 2001.
- Hinds, W. C.: *Aerosol Technology: Properties, Behavior, and Measurement of Airborne Particles*, John Wiley & Sons, New York, 1999.

An improved dust emission model

J. F. Kok et al.

[Title Page](#)[Abstract](#)[Introduction](#)[Conclusions](#)[References](#)[Tables](#)[Figures](#)[◀](#)[▶](#)[◀](#)[▶](#)[Back](#)[Close](#)[Full Screen / Esc](#)[Printer-friendly Version](#)[Interactive Discussion](#)

- Ho, T. D., Valance, A., Dupont, P., and El Moctar, A. O.: Scaling laws in aeolian sand transport, *Phys. Rev. Lett.*, 106, 094501, doi:10.1103/PhysRevLett.106.094501, 2011.
- Holben, B. N., Eck, T. F., Slutsker, I., Tanre, D., Buis, J. P., Setzer, A., Vermote, E., Reagan, J. A., Kaufman, Y. J., Nakajima, T., Lavenu, F., Jankowiak, I., and Smirnov, A.: AERONET – a federated instrument network and data archive for aerosol characterization, *Remote Sens. Environ.*, 66, 1–16, 1998.
- Huneeus, N., Schulz, M., Balkanski, Y., Griesfeller, J., Prospero, J., Kinne, S., Bauer, S., Boucher, O., Chin, M., Dentener, F., Diehl, T., Easter, R., Fillmore, D., Ghan, S., Ginoux, P., Grini, A., Horowitz, L., Koch, D., Krol, M. C., Landing, W., Liu, X., Mahowald, N., Miller, R., Morcrette, J.-J., Myhre, G., Penner, J., Perlwitz, J., Stier, P., Takemura, T., and Zender, C. S.: Global dust model intercomparison in AeroCom phase I, *Atmos. Chem. Phys.*, 11, 7781–7816, doi:10.5194/acp-11-7781-2011, 2011.
- Iversen, J. D. and White, B. R.: Saltation threshold on Earth, Mars and Venus, *Sedimentology*, 29, 111–119, 1982.
- Jansen, E., Overpeck, J., Briffa, K. R., Duplessy, J.-C., Joos, F., Masson-Delmotte, V., Olago, D., Otto-Bliesner, B., Peltier, W. R., Rahmstorf, S., Ramesh, R., Raynaud, D., Rind, D., Solomina, O., Villalba, R., and Zhang, D.: Palaeoclimate, in: *Climate Change 2007: the Physical Science Basis, Contribution of Working Group I to the Fourth Assessment Report of the Intergovernmental Panel on Climate Change*, edited by: Solomon, S., Qin, D., Manning, M., Chen, Z., Marquis, M., Averyt, K. B., Tignor, M., and Miller, H. L., Cambridge University Press, Cambridge, UK and New York, NY, USA, 433–497, 2007.
- Kaaden, N., Massling, A., Schladitz, A., Muller, T., Kandler, K., Schutz, L., Weinzierl, B., Petzold, A., Tesche, M., Leinert, S., Deutscher, C., Ebert, M., Weinbruch, S., and Wiedensohler, A.: State of mixing, shape factor, number size distribution, and hygroscopic growth of the Saharan anthropogenic and mineral dust aerosol at Tinfou, Morocco, *Tellus B*, 61, 51–63, 2009.
- Kaimal, J. C. and Finnigan, J. J.: *Atmospheric boundary layer flows: Their structure and measurement* Oxford Univ. Press, New York, 1994.
- Kallenberg, O.: *Foundations of Modern Probability*, Springer-Verlag, New York, 1997.
- Klose, M. and Shao, Y.: Stochastic parameterization of dust emission and application to convective atmospheric conditions, *Atmos. Chem. Phys.*, 12, 7309–7320, doi:10.5194/acp-12-7309-2012, 2012.

An improved dust emission model

J. F. Kok et al.

Title Page

Abstract

Introduction

Conclusions

References

Tables

Figures

◀

▶

◀

▶

Back

Close

Full Screen / Esc

Printer-friendly Version

Interactive Discussion



- Kohfeld, K. E. and Harrison, S. P.: DIRTMAP: the geological record of dust, *Earth-Sci. Rev.*, 54, 81–114, 2001.
- Kok, J. F.: An improved parameterization of wind-blown sand flux on Mars that includes the effect of hysteresis, *Geophys. Res. Lett.*, 37, L12202, doi:10.1029/2010GL043646, 2010.
- 5 Kok, J. F.: Does the size distribution of mineral dust aerosols depend on the wind speed at emission?, *Atmos. Chem. Phys.*, 11, 10149–10156, doi:10.5194/acp-11-10149-2011, 2011.
- Kok, J. F.: A scaling theory for the size distribution of emitted dust aerosols suggests climate models underestimate the size of the global dust cycle, *P. Natl. Acad. Sci. USA*, 108, 1016–1021, 2011b.
- 10 Kok, J. F. and Renno, N. O.: Enhancement of the emission of mineral dust aerosols by electric forces, *Geophys. Res. Lett.*, 33, L19S10, doi:10.1029/2006GL026284, 2006.
- Kok, J. F., Parteli, E. J. R., Michaels, T. I., and Karam, D. B.: The physics of wind-blown sand and dust, *Rep. Prog. Phys.*, 75, 106901, doi:10.1088/0034-4885/75/10/106901, 2012.
- Kok, J. F. and Renno, N. O.: A comprehensive numerical model of steady state saltation (COM-SALT), *J. Geophys. Res.-Atmos.*, 114, D17204, doi:10.1029/2009JD011702, 2009.
- 15 Koven, C. D. and Fung, I.: Identifying global dust source areas using high-resolution land surface form, *J. Geophys. Res.-Atmos.*, 113, D22204, doi:10.1029/2008JD010195, 2008.
- Kun, F. and Herrmann, H. J.: Transition from damage to fragmentation in collision of solids, *Phys. Rev. E*, 59, 2623–2632, 1999.
- 20 Lawrence, D. M., Oleson, K. W., Flanner, M. G., Thornton, P. E., Swenson, S. C., Lawrence, P. J., Zeng, X. B., Yang, Z. L., Levis, S., Sakaguchi, K., Bonan, G. B., and Slater, A. G.: Parameterization Improvements and Functional and Structural Advances in Version 4 of the Community Land Model, *J. Adv. Model. Earth Syst.*, 3, M03001, doi:10.1029/2011MS000045, 2011.
- 25 Liu, X., Easter, R. C., Ghan, S. J., Zaveri, R., Rasch, P., Shi, X., Lamarque, J.-F., Gettelman, A., Morrison, H., Vitt, F., Conley, A., Park, S., Neale, R., Hannay, C., Ekman, A. M. L., Hess, P., Mahowald, N., Collins, W., Iacono, M. J., Bretherton, C. S., Flanner, M. G., and Mitchell, D.: Toward a minimal representation of aerosols in climate models: description and evaluation in the Community Atmosphere Model CAM5, *Geosci. Model Dev.*, 5, 709–739, doi:10.5194/gmd-5-709-2012, 2012.
- 30 Ma, P.-L., Rasch, P. J., Wang, H., Zhang, K., Easter, R. C., Tilmes, S., Fast, J. D., Liu, X., Yoon, J.-H., and Lamarque, J.-F.: The role of circulation features on black carbon transport

An improved dust emission model

J. F. Kok et al.

Title Page

Abstract

Introduction

Conclusions

References

Tables

Figures

◀

▶

◀

▶

Back

Close

Full Screen / Esc

Printer-friendly Version

Interactive Discussion



into the Arctic in the Community Atmosphere Model version 5 (CAM5), *J. Geophys. Res.-Atmos.*, 118, 4657–4669, 2013.

Mahowald, N. M. and Dufresne, J. L.: Sensitivity of TOMS aerosol index to boundary layer height: implications for detection of mineral aerosol sources, *Geophys. Res. Lett.*, 31, L03103, doi:10.1029/2003GL018865, 2004.

Mahowald, N. M., Zender, C. S., Luo, C., Savoie, D., Torres, O., and del Corral, J.: Understanding the 30-year Barbados desert dust record, *J. Geophys. Res.-Atmos.*, 107, 4561, doi:10.1029/2002JD002097, 2002.

Mahowald, N. M., Lamarque, J. F., Tie, X. X., and Wolff, E.: Sea-salt aerosol response to climate change: Last Glacial Maximum, preindustrial, and doubled carbon dioxide climates, *J. Geophys. Res.-Atmos.*, 111, 4561, doi:10.1029/2002JD002097, 2006a.

Mahowald, N. M., Muhs, D. R., Levis, S., Rasch, P. J., Yoshioka, M., Zender, C. S., and Luo, C.: Change in atmospheric mineral aerosols in response to climate: Last glacial period, preindustrial, modern, and doubled carbon dioxide climates, *J. Geophys. Res.*, 111, D10202, doi:10.1029/2005JD006653, 2006b.

Mahowald, N. M., Kloster, S., Engelstaedter, S., Moore, J. K., Mukhopadhyay, S., McConnell, J. R., Albani, S., Doney, S. C., Bhattacharya, A., Curran, M. A. J., Flanner, M. G., Hoffman, F. M., Lawrence, D. M., Lindsay, K., Mayewski, P. A., Neff, J., Rothenberg, D., Thomas, E., Thornton, P. E., and Zender, C. S.: Observed 20th century desert dust variability: impact on climate and biogeochemistry, *Atmos. Chem. Phys.*, 10, 10875–10893, doi:10.5194/acp-10-10875-2010, 2010.

Martcorena, B. and Bergametti, G.: Modeling the atmospheric dust cycle .1. Design of a soil-derived emission scheme, *J. Geophys. Res.-Atmos.*, 100, 16415–16430, 1995.

Martcorena, B., Chazette, P., Bergametti, G., Dulac, F., and Legrand, M.: Mapping the aerodynamic roughness length of desert surfaces from the POLDER/ADEOS bi-directional reflectance product, *Int. J. Remote Sens.*, 25, 603–626, 2004.

Martin, J. H., Gordon, R. M., and Fitzwater, S. E.: The case for iron, *Limnol. Oceanogr.*, 36, 1793–1802, 1991.

Martin, R. L., Barchyn, T. E., Hugenholtz, C. H., and Jerolmack, D. J.: Timescale dependence of aeolian sand flux observations under atmospheric turbulence, *J. Geophys. Res.-Atmos.*, 118, 9078–9092, 2013.

An improved dust emission model

J. F. Kok et al.

Title Page

Abstract

Introduction

Conclusions

References

Tables

Figures

◀

▶

◀

▶

Back

Close

Full Screen / Esc

Printer-friendly Version

Interactive Discussion



McKenna Neuman, C. and Nickling, W. G.: A theoretical and wind-tunnel investigation of the effect of capillary water on the entrainment of sediment by wind, *Can. J. Soil Sci.*, 69, 79–96, 1989.

Miller, R. L. and Tegen, I.: Climate response to soil dust aerosols, *J. Climate*, 11, 3247–3267, 1998.

Mokhtari, M., Gomes, L., Tulet, P., and Rezoug, T.: Importance of the surface size distribution of erodible material: an improvement on the Dust Entrainment And Deposition (DEAD) Model, *Geosci. Model Dev.*, 5, 581–598, doi:10.5194/gmd-5-581-2012, 2012.

Namikas, S. L., Bauer, B. O., and Sherman, D. J.: Influence of averaging interval on shear velocity estimates for aeolian transport modeling, *Geomorphology*, 53, 235–246, 2003.

Neale, R. B., Chen, C.-C., Gettelman, A., Lauritzen, P. H., Park, S. U., Williamson, D. L., Conley, A. J., Garcia, R., Kinnison, D., Lamarque, J. F., Marsh, D., Mills, M., Smith, A. K., Tilmes, S., Vitt, F., Morrison, H., Cameron-Smith, P., Collins, W. D., Jacono, M. J., Easter, R. C., Ghan, S. J., Liu, X., Rasch, P. J., and Taylor, M. A.: Description of the NCAR Community Atmosphere Model (CAM 5.0), NCAR Technical Note, TN-486, Boulder, CO, 268 pp., 2010.

Nickling, W. G.: Eolian sediment transport during dust storms – Slims river valley, Yukon territory, *Can. J. Earth Sci.*, 15, 1069–1084, 1978.

Nickling, W. G.: Grain-size characteristics of sediment transported during dust storms, *J. Sediment. Petrol.*, 53, 1011–1024, 1983.

Nickling, W. G. and Gillies, J. A.: Dust emission and transport in Mali, West-Africa, *Sedimentology*, 40, 859–868, 1993.

Nickling, W. G. and McKenna Neuman, C.: Aeolian sediment transport, in: *Geomorphology of Desert Environments*, edited by: Parsons, A. J. and Abrahams, A. D. (Eds.), Springer Science+Business Media, New York, 517–555, 2009.

Nickling, W. G., McTainsh, G. H., and Leys, J. F.: Dust emissions from the Channel Country of western Queensland, Australia, *Z. Geomorphol. Supp.*, 116, 1–17, 1999.

O'Brien, P. and McKenna Neuman, C.: A wind tunnel study of particle kinematics during crust rupture and erosion, *Geomorphology*, 173, 149–160, 2012.

Oger, L., Ammi, M., Valance, A., and Beladjine, D.: Study of the collision of one rapid sphere on 3D packings: experimental and numerical results, *Comput. Math. Appl.*, 55, 132–148, 2008.

Oleson, K. W., Lawrence, D. M., Gordon, B. B., Flanner, M. G., Kluzek, E., Lawrence, P. J., Levis, S., Swenson, S. C., Thornton, P. E., Dai, A., Decker, M., Dickinson, R., Feddema, J.,

An improved dust emission model

J. F. Kok et al.

Title Page

Abstract

Introduction

Conclusions

References

Tables

Figures

◀

▶

◀

▶

Back

Close

Full Screen / Esc

Printer-friendly Version

Interactive Discussion



Heald, C. L., Hoffman, F., Lamarque, J.-F., Mahowald, N., Niu, G.-Y., Qian, T., Randerson, J., Running, S., Sakaguchi, K., Slater, A., Stockli, R., Wang, A., Yang, Z.-L., Zeng, Z., and Zeng, X.: Technical Description of version 4.0 of the Community Land Model (CLM), NCAR Technical Note, TN-478, 257 pp., Boulder, CO, 2010.

5 Owen, P. R.: Saltation of uniform grains in air, *J. Fluid Mech.*, 20, 225–242, 1964.

Park, M. S., Park, S. U., and Chun, Y.: Improved parameterization of dust emission (PM_{10}) fluxes by the gradient method using the Naiman tower data at the Horqin desert in China, *Sci. Total. Environ.*, 412, 265–277, 2011.

10 Prospero, J. M. and Lamb, P. J.: African droughts and dust transport to the Caribbean: climate change implications, *Science*, 302, 1024–1027, 2003.

Prospero, J. M. and Nees, R. T.: Impact of the north african drought and el-nino on mineral dust in the barbados trade winds, *Nature*, 320, 735–738, 1986.

15 Prospero, J. M., Ginoux, P., Torres, O., Nicholson, S. E., and Gill, T. E.: Environmental characterization of global sources of atmospheric soil dust identified with the Nimbus 7 Total Ozone Mapping Spectrometer (TOMS) absorbing aerosol product, *Rev. Geophys.*, 40, 1002, doi:10.1029/2000RG000095, 2002.

Rasmussen, K. R. and Sorensen, M.: Aeolian mass transport near the saltation threshold, *Earth Surf. Proc. Land.*, 24, 413–422, 1999.

20 Raupach, M. R., Gillette, D. A., and Leys, J. F.: The effect of roughness elements on wind erosion threshold, *J. Geophys. Res.-Atmos.*, 98, 3023–3029, 1993.

Ravi, S., D'Odorico, P., Over, T. M., and Zobeck, T. M.: On the effect of air humidity on soil susceptibility to wind erosion: the case of air-dry soils, *Geophys. Res. Lett.*, 31, L09501, doi:10.1029/2004GL019485, 2004.

25 Ravi, S., Zobeck, T. M., Over, T. M., Okin, G. S., and D'Odorico, P.: On the effect of moisture bonding forces in air-dry soils on threshold friction velocity of wind erosion, *Sedimentology*, 53, 597–609, 2006.

Rea, D. K.: The paleoclimatic record provided by eolian deposition in the deep-sea – the geologic history of wind, *Rev. Geophys.*, 32, 159–195, 1994.

30 Reid, J. S., Jonsson, H. H., Maring, H. B., Smirnov, A., Savoie, D. L., Cliff, S. S., Reid, E. A., Livingston, J. M., Meier, M. M., Dubovik, O., and Tsay, S. C.: Comparison of size and morphological measurements of coarse mode dust particles from Africa, *J. Geophys. Res.-Atmos.*, 108, 8593, doi:10.1029/2002JD002485, 2003.

An improved dust emission model

J. F. Kok et al.

Title Page

Abstract

Introduction

Conclusions

References

Tables

Figures

◀

▶

◀

▶

Back

Close

Full Screen / Esc

Printer-friendly Version

Interactive Discussion



- Rice, M. A., Willetts, B. B., and McEwan, I. K.: Observations of collisions of saltating grains with a granular bed from high-speed cine-film, *Sedimentology*, 43, 21–31, 1996.
- Rice, M. A., McEwan, I. K., and Mullins, C. E.: A conceptual model of wind erosion of soil surfaces by saltating particles, *Earth Surf. Proc. Land.*, 24, 383–392, 1999.
- 5 Schepanski, K., Tegen, I., Todd, M. C., Heinold, B., Bonisch, G., Laurent, B., and Macke, A.: Meteorological processes forcing Saharan dust emission inferred from MSG-SEVIRI observations of subdaily dust source activation and numerical models, *J. Geophys. Res.-Atmos.*, 114, D10201, doi:10.1029/2008JD010325, 2009.
- Shao, Y.: A model for mineral dust emission, *J. Geophys. Res.-Atmos.*, 106, 20239–20254, 2001.
- 10 Shao, Y., Ishizuka, M., Mikami, M., and Leys, J. F.: Parameterization of size-resolved dust emission and validation with measurements, *J. Geophys. Res.-Atmos.*, 116, D08203, doi:10.1029/2010JD014527, 2011.
- Shao, Y. P.: *Physics and Modelling of Wind Erosion*, Springer, Heidelberg, 2008.
- 15 Shao, Y. P. and Li, A.: Numerical modelling of saltation in the atmospheric surface layer, *Bound.-Lay. Meteorol.*, 91, 199–225, 1999.
- Shao, Y. P. and Lu, H.: A simple expression for wind erosion threshold friction velocity, *J. Geophys. Res.-Atmos.*, 105, 22437–22443, 2000.
- Shao, Y. P., Raupach, M. R., and Findlater, P. A.: Effect of saltation bombardment on the entrainment of dust by wind, *J. Geophys. Res.-Atmos.*, 98, 12719–12726, 1993.
- 20 Shao, Y. P., Raupach, M. R., and Leys, J. F.: A model for predicting aeolian sand drift and dust entrainment on scales from paddock to region, *Aust. J. Soil Res.*, 34, 309–342, 1996.
- Sherman, D. J. and Farrell, E. J.: Aerodynamic roughness lengths over movable beds: Comparison of wind tunnel and field data, *J. Geophys. Res.-Earth*, 113, F02S08, doi:10.1029/2007JF000784, 2008.
- 25 Solomon, S., Qin, D., Manning, M., Alley, R. B., Berntsen, T., Bindoff, Z., Chen, Z., Chidthaisong, A., Gregory, J. M., Hegerl, G. C., Heimann, M., Hewitson, B., Hoskins, B. J., Joos, F., Jouzel, J., Kattsov, V., Lohmann, U., Matsuno, T., Molina, M., Nicholls, N., Overpeck, J., Raga, G., Ramaswamy, V., Ren, J., Rusticucci, M., Somerville, R., Stocker, T. F., Whetton, P., Wood, R. A., and Wratt, D.: Technical Summary, in: *Climate Change 2007: The Physical Science Basis. Contribution of Working Group I to the Fourth Assessment Report of the Intergovernmental Panel on Climate Change*, edited by: Solomon, S., Qin, D.,
- 30

An improved dust emission model

J. F. Kok et al.

Title Page

Abstract

Introduction

Conclusions

References

Tables

Figures

◀

▶

◀

▶

Back

Close

Full Screen / Esc

Printer-friendly Version

Interactive Discussion



Manning, M., Chen, Z., Marquis, M., Averyt, K. B., Tignor, M., and Miller, H. L., Cambridge University Press, Cambridge, UK and New York, NY, USA, 2007.

Sow, M., Alfaro, S. C., Rajot, J. L., and Marticorena, B.: Size resolved dust emission fluxes measured in Niger during 3 dust storms of the AMMA experiment, *Atmos. Chem. Phys.*, 9, 3881–3891, doi:10.5194/acp-9-3881-2009, 2009.

Stockton, P. H. and Gillette, D. A.: Field measurement of the sheltering effect of vegetation on erodible land surfaces, *Land Degrad. Rehabil.*, 2, 77–85, 1990.

Sweeney, M. R. and Mason, J. A.: Mechanisms of dust emission from Pleistocene loess deposits, Nebraska, USA, *J. Geophys. Res.*, 118, 1460–1471, 2013.

Tegen, I., Harrison, S. P., Kohfeld, K., Prentice, I. C., Coe, M., and Heimann, M.: Impact of vegetation and preferential source areas on global dust aerosol: results from a model study, *J. Geophys. Res.-Atmos.*, 107, 4576, doi:10.1029/2001JD000963, 2002.

Tegen, I., Werner, M., Harrison, S. P., and Kohfeld, K. E.: Relative importance of climate and land use in determining present and future global soil dust emission, *Geophys. Res. Lett.*, 31, L05105, doi:10.1029/2003GL019216, 2004.

Ungar, J. E. and Haff, P. K.: Steady-state saltation in air, *Sedimentology*, 34, 289–299, 1987.

van Boxel, J. H., Sterk, G., and Arens, S. M.: Sonic anemometers in aeolian sediment transport research, *Geomorphology*, 59, 131–147, 2004.

van Donk, S. J., Huang, X. W., Skidmore, E. L., Anderson, A. B., Gebhart, D. L., Prehoda, V. E., and Kellogg, E. M.: Wind erosion from military training lands in the Mojave Desert, California, USA, *J. Arid Environ.*, 54, 687–703, 2003.

Videen, G. and Chylek, P.: Scattering by a composite sphere with an absorbing inclusion and effective medium approximations, *Opt. Commun.*, 158, 1–6, 1998.

Washington, R., Bouet, C., Cautenet, G., Mackenzie, E., Ashpole, I., Engelstaedter, S., Lizcano, G., Henderson, G. M., Schepanski, K., and Tegen, I.: Dust as a tipping element: The Bodele Depression, Chad, *P. Natl. Acad. Sci. USA*, 106, 20564–20571, 2009.

Werner, M., Tegen, I., Harrison, S. P., Kohfeld, K. E., Prentice, I. C., Balkanski, Y., Rodhe, H., and Roelandt, C.: Seasonal and interannual variability of the mineral dust cycle under present and glacial climate conditions, *J. Geophys. Res.-Atmos.*, 107, 4744, doi:10.1029/2002JD002365, 2002.

Wiggs, G. F. S., Atherton, R. J., and Baird, A. J.: Thresholds of aeolian sand transport: establishing suitable values, *Sedimentology*, 51, 95–108, 2004.

Zender, C. S., Bian, H. S., and Newman, D.: Mineral Dust Entrainment and Deposition (DEAD) model: Description and 1990s dust climatology, *J. Geophys. Res.-Atmospheres*, 108, 4416, doi:10.1029/2002JD002775, 2003a.

Zender, C. S., Newman, D., and Torres, O.: Spatial heterogeneity in aeolian erodibility: Uniform, topographic, geomorphic, and hydrologic hypotheses, *J. Geophys. Res.-Atmos.*, 108, 4543, doi:10.1029/2002JD003039, 2003b.

Zobeck, T. M.: Soil properties affecting wind erosion, *J. Soil Water Conserv.*, 46, 112–118, 1991.

Zobeck, T. M. and Van Pelt, R. S.: Wind-induced dust generation and transport mechanics on a bare agricultural field, *J. Hazard. Mater.*, 132, 26–38, 2006.

ACPD

14, 6361–6425, 2014

An improved dust emission model

J. F. Kok et al.

Title Page

Abstract

Introduction

Conclusions

References

Tables

Figures

◀

▶

◀

▶

Back

Close

Full Screen / Esc

Printer-friendly Version

Interactive Discussion



An improved dust emission model

J. F. Kok et al.

Table 2. Root mean square error (RMSE) of the vertical dust flux predicted by the parameterizations of Gillette and Passi (1988) (denoted as GP88), Marticorena and Bergametti (1995) (MB95), and Eq. (19). RMSE values were calculated for three separate cases. For the first case, the proportionality constant was tuned to a single value that minimized the mean RMSE for all data sets. The resulting RMSE for this case is thus a measure of the parameterization's ability to reproduce variations in the dust flux due to variations in both u_* and soil conditions (u_{*t} and f_{clay}). For the second case, the proportionality constant in each parameterization was tuned separately for each data set. The resulting RMSE is thus a measure of a parameterization's ability to reproduce the dust flux's dependence on u_* for each individual data set. For the third case, all dimensionless constants in each parameterization were tuned to minimize the mean RMSE for all data sets (see text). All RMSEs were calculated in log10-space such that each data point was weighted equally, and the lowest RMSE for the three different parameterizations is underlined for each case.

| Study | Event | GP88, Case 1 ^a | MB95, Case 1 ^a | Eq. (19), Case 1 | GP88, Case 2 ^b | MB95, Case 2 ^b | Eq. (19), Case 2 ^b | GP88, Case 3 ^c | MB95, Case 3 ^c | Eq. (19), Case 3 ^c |
|----------------|---------|---------------------------|---------------------------|---------------------|---------------------------|---------------------------|-------------------------------|---------------------------|---------------------------|-------------------------------|
| GB04 | 16 Feb | 0.400 | <u>0.383</u> | 0.682 | 0.203 | <u>0.181</u> | 0.182 | 0.381 | <u>0.322</u> | 0.800 |
| GB04 | 20 Mar | 0.247 | 0.195 | <u>0.130</u> | 0.112 | 0.108 | <u>0.103</u> | <u>0.133</u> | 0.143 | 0.186 |
| ZP06 | 4 Mar | 1.043 | 1.482 | <u>0.365</u> | 0.306 | 0.325 | <u>0.297</u> | 0.775 | 0.793 | <u>0.400</u> |
| ZP06 | 18 Mar | 0.390 | 0.908 | <u>0.115</u> | 0.088 | 0.111 | <u>0.085</u> | 0.233 | 0.263 | <u>0.089</u> |
| FC07 | Event 1 | – | – | – | 0.377 | 0.155 | <u>0.146</u> | – | – | – |
| FC07 | Event 2 | – | – | – | 0.389 | 0.192 | <u>0.132</u> | – | – | – |
| SA09 | ME1 | <u>0.299</u> | 0.957 | 0.364 | <u>0.054</u> | 0.072 | 0.056 | <u>0.159</u> | 0.160 | 0.225 |
| SA09 | CE4 | <u>0.387</u> | 1.175 | 0.504 | <u>0.104</u> | 0.114 | 0.110 | <u>0.368</u> | 0.419 | 0.387 |
| SI11 | N/A | 1.286 | 0.731 | <u>0.101</u> | 0.161 | 0.107 | <u>0.099</u> | 0.873 | 0.859 | <u>0.198</u> |
| PP11 | Event 1 | – | – | – | 0.609 | 0.347 | <u>0.294</u> | – | – | – |
| PP11 | Event 2 | – | – | – | 0.656 | 0.356 | <u>0.329</u> | – | – | – |
| Average | | <u>0.579</u> | <u>0.833</u> | <u>0.323</u> | <u>0.278</u> | <u>0.188</u> | <u>0.167</u> | 0.410 | 0.412 | <u>0.316</u> |

^a Parameterization's proportionality constant tuned separately to a value that minimizes the RMSE for each data set.

^b Parameterization's proportionality constant tuned to a single value that minimizes the RMSE for all data sets.

^c All the parameterization's dimensionless constants are tuned to a single value that minimizes the RMSE for all data sets.

Title Page

Abstract

Introduction

Conclusions

References

Tables

Figures

◀

▶

◀

▶

Back

Close

Full Screen / Esc

Printer-friendly Version

Interactive Discussion



An improved dust emission model

J. F. Kok et al.

Title Page

Abstract

Introduction

Conclusions

References

Tables

Figures

I ◀

▶ I

◀

▶

Back

Close

Full Screen / Esc

Printer-friendly Version

Interactive Discussion



Table 3. Summary of CESM simulations used in this study, and the statistics of their comparison against AERONET data. The highest (Pearson) correlation coefficients (r) and the lowest root mean square errors (RMSE) of the four simulations are underlined for clarity.

| Simulation | Dust flux parameterization | Preferential sources function | AERONET correlation coefficient (r) | AERONET RMSE |
|------------|----------------------------|-------------------------------|---|--------------|
| I | MB95 | None | 0.602 | 0.139 |
| II | MB95 | Zender et al. (2003b) | 0.629 | 0.135 |
| III | MB95 | Ginoux et al. (2001) | 0.636 | 0.135 |
| IV | Eq. (19) | None | <u>0.747</u> | <u>0.113</u> |

An improved dust emission model

J. F. Kok et al.

Title Page

Abstract

Introduction

Conclusions

References

Tables

Figures

◀

▶

◀

▶

Back

Close

Full Screen / Esc

Printer-friendly Version

Interactive Discussion



Table 4. Sensitivity of AERONET comparison results for all four simulations to changes in the soil moisture sensitivity tuning parameter b (see Eq. 30). The highest correlation coefficients and the lowest root mean square errors (RMSE) of the four simulations are underlined for each case.

| Soil moisture tuning parameter (b) | Correlation coefficient (Sim. I/II/III/IV) | RMSE (Sim. I/II/III/IV) |
|--|--|--|
| 1 | 0.602/0.629/0.636/ <u>0.747</u> | 0.139/0.135/0.135/ <u>0.113</u> |
| 2 | 0.521/0.524/0.608/ <u>0.650</u> | 0.151/0.150/0.137/ <u>0.128</u> |
| 3 | 0.516/0.520/0.606/ <u>0.645</u> | 0.151/0.151/0.137/ <u>0.129</u> |
| $1/f_{\text{clay}}$ | 0.514/0.519/0.606/ <u>0.643</u> | 0.151/0.151/0.137/ <u>0.129</u> |

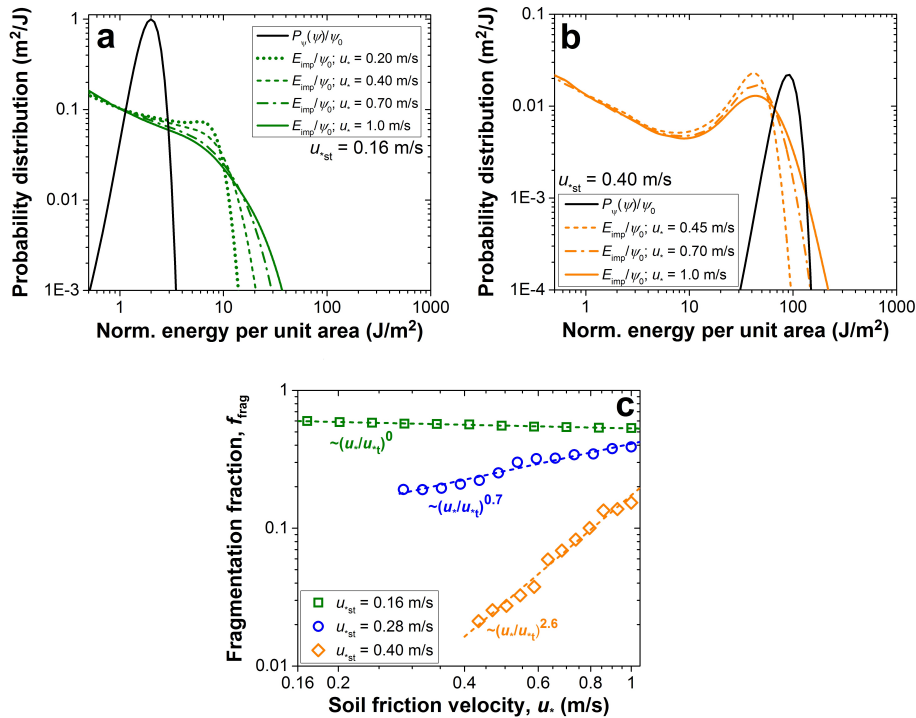


Fig. 1. Probability distributions of the threshold impact energy per unit area (ψ) required for aggregate fragmentation (solid black line), and of the saltator impact energy per unit area (E_{imp}) for different values of u_* (colored lines). Shown are results for (a) a highly erodible soil ($u_{*st} = 0.16 \text{ ms}^{-1}$) and (b) an erosion-resistant soil ($u_{*st} = 0.40 \text{ ms}^{-1}$). The value of f_{frag} increases with u_* for erosion-resistant soils, but not for highly erodible soils, as shown explicitly in (c). All plotted energy values are normalized by ψ_0 , the energy per unit area of a $100 \mu\text{m}$ saltator impacting at 1 ms^{-1} , and $P_\psi(\psi)$ was calculated using $c_\psi = 2$ and $\sigma_\psi = 0.2\bar{\psi}$.

Title Page

Abstract

Introduction

Conclusions

References

Tables

Figures

◀

▶

◀

▶

Back

Close

Full Screen / Esc

Printer-friendly Version

Interactive Discussion



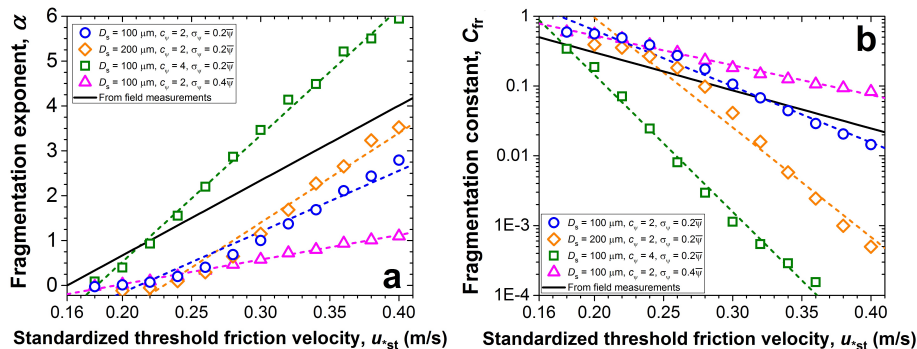


Fig. 2. Simulation of the fragmentation exponent α (a) and constant C_{fr} (b) with the numerical saltation model COMSALT (Kok and Renno, 2009) for different values of the saltating particle size (D_s) and the threshold fragmentation energy's normal distribution parameters (c_ψ and σ_ψ). The colored dashed lines represent the best fits of the functional forms of Eqs. (17) and (18) to the corresponding simulation results, and the solid black lines represents the best fit to the experimental data in Fig. 4.

[Title Page](#)
[Abstract](#)
[Introduction](#)
[Conclusions](#)
[References](#)
[Tables](#)
[Figures](#)
[◀](#)
[▶](#)
[◀](#)
[▶](#)
[Back](#)
[Close](#)
[Full Screen / Esc](#)
[Printer-friendly Version](#)
[Interactive Discussion](#)


An improved dust emission model

J. F. Kok et al.

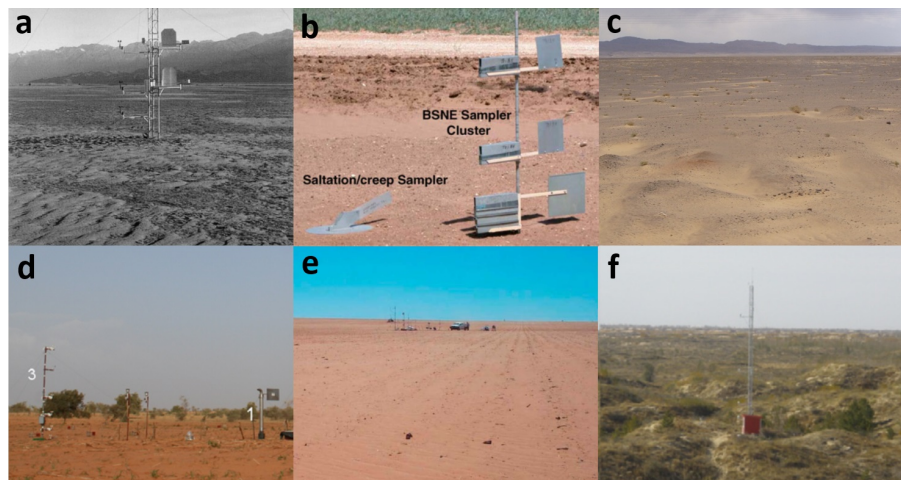


Fig. 3. The experimental field sites of the 6 studies in our vertical dust flux compilation: **(a)** Gillies and Berkofsky (2004) (36.48° N, 117.90° W), **(b)** Zobeck and Van Pelt (2006) (32.27° N, 101.49° W), **(c)** Fratini et al. (2007) (100.54° E, 41.88° N), **(d)** Sow et al. (2009) (13.5° N, 2.6° E), **(e)** Shao et al. (2011) (33.85° S, 142.74° E), and **(f)** Park et al. (2011) (42.93° N, 120.70° E).

Title Page

Abstract

Introduction

Conclusions

References

Tables

Figures

I◀

▶I

◀

▶

Back

Close

Full Screen / Esc

Printer-friendly Version

Interactive Discussion



An improved dust emission model

J. F. Kok et al.

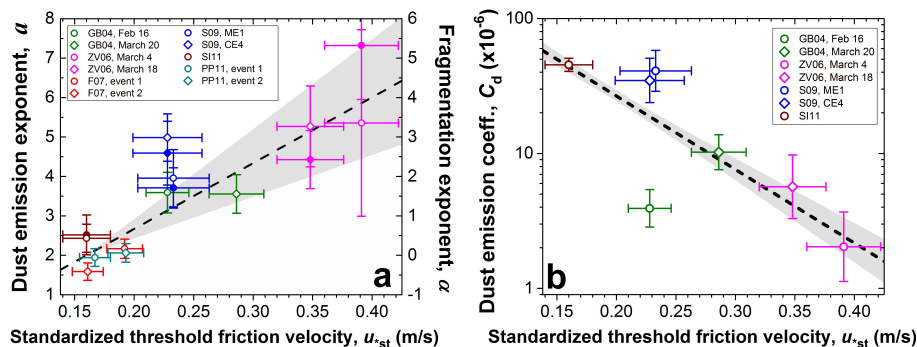


Fig. 4. Values of **(a)** the dust emission exponent α ($= \alpha + 2$) and **(b)** the dust emission coefficient C_d as a function of the standardized threshold friction velocity u_{*st} , determined from the analysis of available quality-controlled data sets. Open symbols refer to estimates of C_d and α from the least-squares fit of the measured dust flux to Eq. (19), whereas filled symbols refer to estimates of α from a least-squares fit to ratios of the measured vertical dust flux and the horizontal saltation flux (see text for details). The dashed line indicates the best-fit forms of Eqs. (17) and (19b), and the grey shaded area denotes one standard error from the fitted relation.

Title Page

Abstract

Introduction

Conclusions

References

Tables

Figures

◀

▶

◀

▶

Back

Close

Full Screen / Esc

Printer-friendly Version

Interactive Discussion



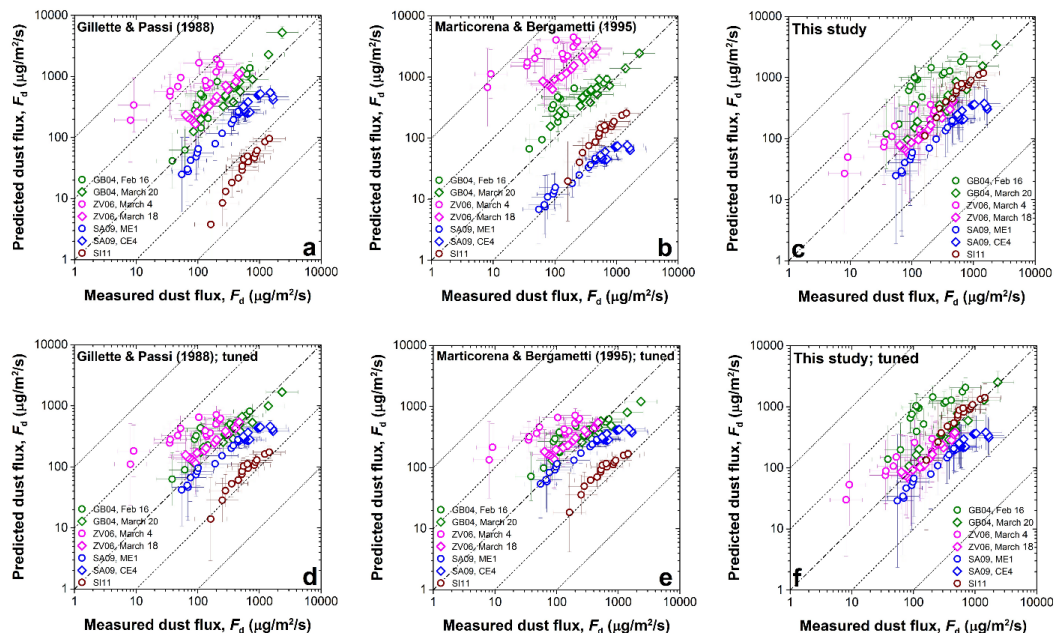


Fig. 5. Comparison of measured dust fluxes with the predictions of the parameterizations of **(a, b)** Gillette and Passi (1988), **(c, d)** Marticorena and Bergametti (1995), and **(e, f)** this study. The proportionality constant in each parameterization was adjusted to maximize agreement with the compilation of measurements. For the top panels, other coefficients in each parameterization are as given in the original study (and as listed in Sect. 3.4 for panel **(c)**). For the bottom panels, all coefficients in each parameterization are tuned to minimize the RMSE with all data sets (see text). To prevent cluttering of the graph, only 15 representative measurements are shown for each data set. Error bars denote uncertainty arising from the measurement of u_{*t} , u_{*s} and F_d (see the Supplement). Data set names are as defined in Sect. 3.1.

An improved dust emission model

J. F. Kok et al.

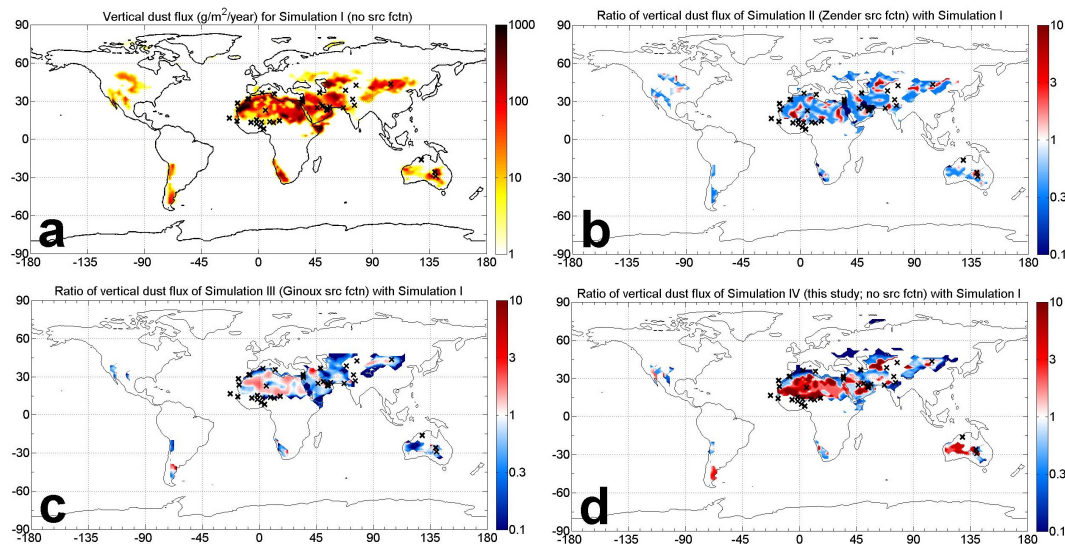


Fig. 6. Global maps of (a) the simulated vertical dust flux for Simulation I and (b–d) the ratios of dust flux in Simulations II–IV to the flux in Simulation I. Red coloring denotes increases in dust emission flux relative to the “control” (Simulation I). The locations of the AERONET stations used for the analysis in Fig. 8 are marked with black crosses.

[Title Page](#)[Abstract](#)[Introduction](#)[Conclusions](#)[References](#)[Tables](#)[Figures](#)[◀](#)[▶](#)[◀](#)[▶](#)[Back](#)[Close](#)[Full Screen / Esc](#)[Printer-friendly Version](#)[Interactive Discussion](#)

An improved dust emission model

J. F. Kok et al.

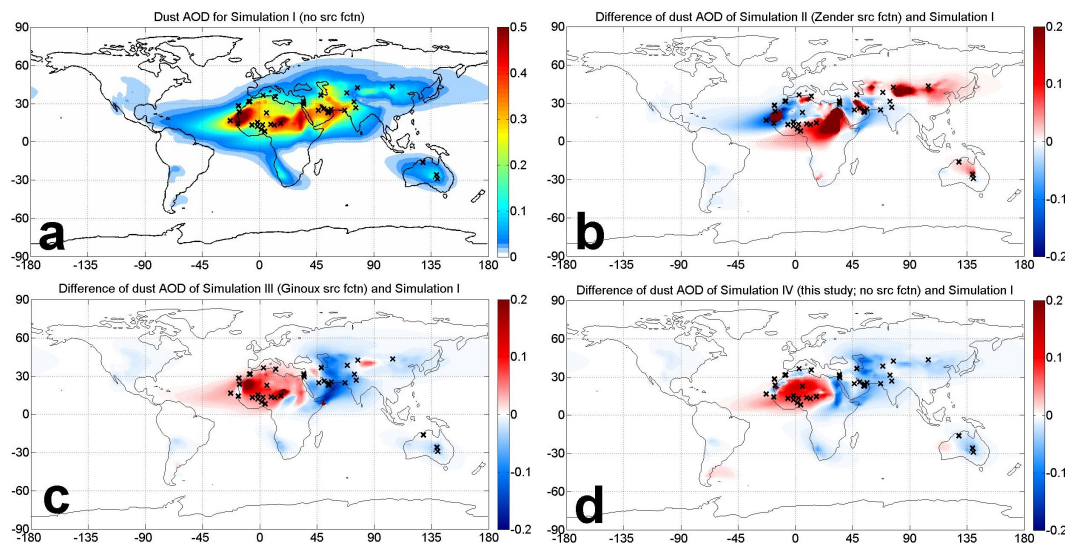


Fig. 7. Global maps of (a) the dust aerosol optical depth (AOD) of Simulation I, and (b–d) the difference of dust AOD of Simulations II–IV with that of Simulation I. Red shading denotes increases in dust AOD relative to the “control” (Simulation I). The locations of the AERONET stations used for the analysis in Fig. 8 are marked with black crosses.

Title Page

Abstract

Introduction

Conclusions

References

Tables

Figures

◀

▶

◀

▶

Back

Close

Full Screen / Esc

Printer-friendly Version

Interactive Discussion



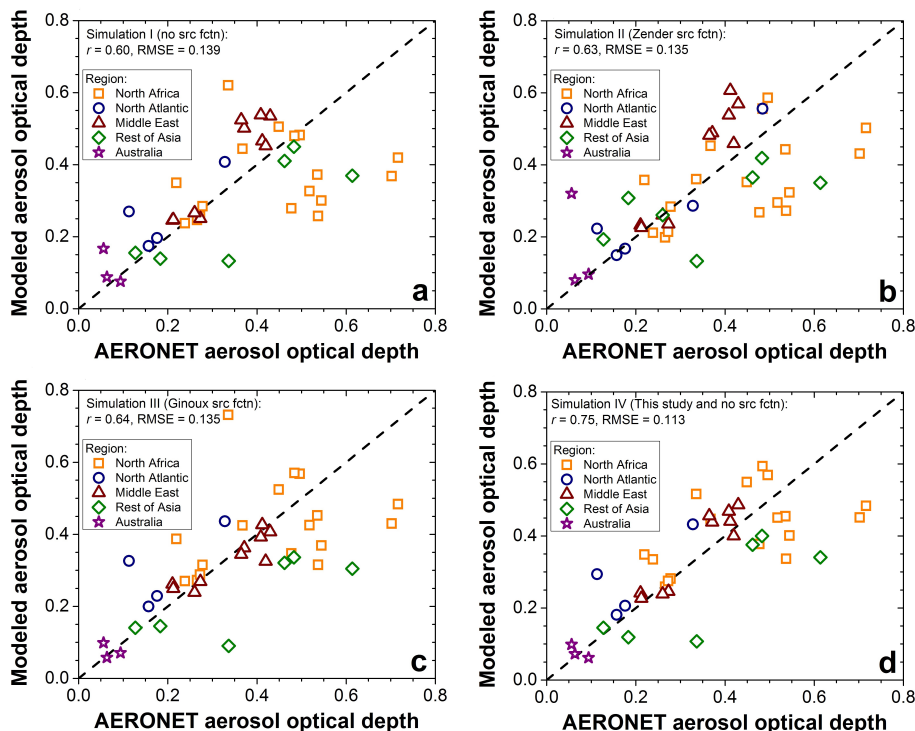


Fig. 8. Comparison of measured and modeled aerosol optical depth at dust-dominated AERONET stations. Results are shown for (a) Simulation I (no source function), (b) Simulation II (Zender et al. (2003b) source function), (c) Simulation III (Ginoux et al. (2001) source function), and (d) Simulation IV (no source function, and dust flux is parameterized using Eq. (19) instead of following MB95). For each simulation, the root mean square error (RMSE) and correlation coefficient (r) are noted.

[Title Page](#)
[Abstract](#)
[Introduction](#)
[Conclusions](#)
[References](#)
[Tables](#)
[Figures](#)
[◀](#)
[▶](#)
[◀](#)
[▶](#)
[Back](#)
[Close](#)
[Full Screen / Esc](#)
[Printer-friendly Version](#)
[Interactive Discussion](#)

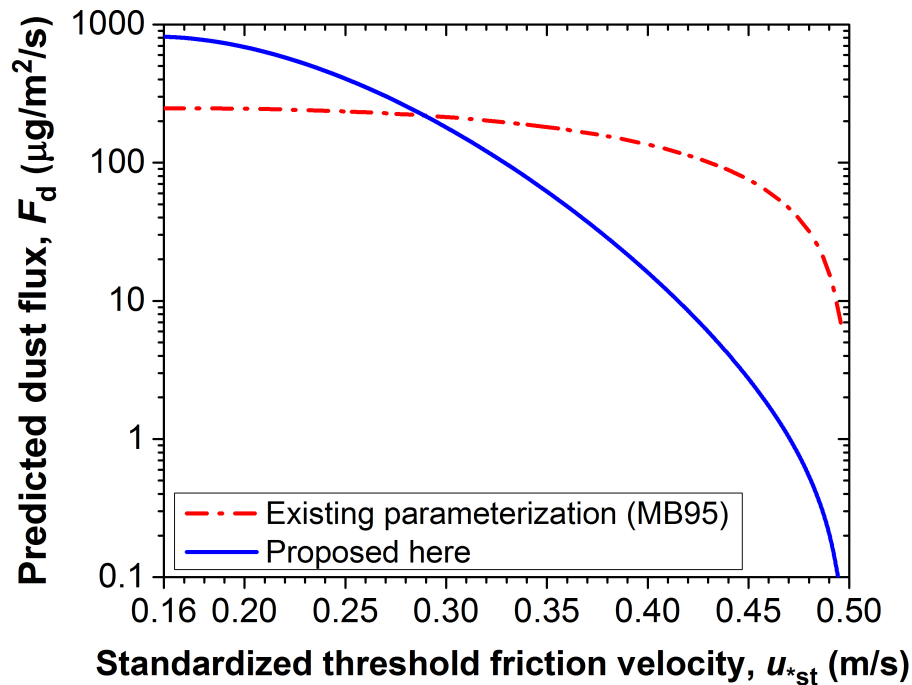



Fig. 9. The vertical dust flux (F_d) as a function of the soil's standardized threshold friction velocity (u_{*st}) in CLM4 for the parameterization proposed here (Eq. 19; solid blue line) and for the existing dust flux parameterization, which follows MB95 (dash-dotted red line; see Zender et al. (2003a)). Results are shown for $u_* = 0.50 \text{ ms}^{-1}$ and for $f_{\text{clay}} = 15\%$, which is a typical value for dust emitting regions (FAO, 2012). The predicted dust fluxes include a global tuning factor that equalizes the global dust emission rate for the two parameterizations.

An improved dust emission model

J. F. Kok et al.

| | |
|--------------------------|--------------|
| Title Page | |
| Abstract | Introduction |
| Conclusions | References |
| Tables | Figures |
| ◀ | ▶ |
| ◀ | ▶ |
| Back | Close |
| Full Screen / Esc | |
| Printer-friendly Version | |
| Interactive Discussion | |

